Experimental Investigation of Exposed Column Base Plate Connections Subjected to Combined Axial and Bi-Directional Lateral Loading

by

Kyle Roller

A thesis
submitted to the Faculty of Graduate Studies
in partial fulfilment of the requirements for the
Degree of Master of Science
in

Civil Engineering

Supervisors
Dr. Muntasir Billah
Assistant Professor – Dept. of Civil Engineering
Dr. Ahmed Elshaer
Associate Professor – Dept. of Civil Engineering

Lakehead University
Thunder Bay, Ontario
Aug 2023

Author's Declaration Page

I hereby declare that I am the sole author of this thesis. This is a true copy of the thesis, including any required final revisions, as accepted by my examiners. I understand that my thesis may be made electronically available to the public.

Abstract

Column base plate (CBP) connections are critical components in the overall design of a steel structure. CBP connections are responsible for transferring the forces exerted on base columns through a base plate and grout pad into the concrete foundation utilizing anchor rods. Exposed-type column bases are widely used in low-rise building construction all over the world, and considerable research efforts have been made to identify the parameters that affect their strength and serviceability. Current design codes and guidelines do not address the design of these exposed base plate connections under combined axial load and bi-axial bending. Although, the columns are designed and checked under combined axial load and bi-axial bending, when it comes to the base plate connection, only the axial load and major axis bending are considered. Practicing engineers often adopt complex finite element method or design them in two directions separately, which often results in overly conservative design. A more direct approach to designing CBP connections subjected to combined axial and lateral loading conditions would help ensure column base connections perform as intended under extreme loading. The inadequate design of a CBP connection will cause the failure of the connection before the column can reach its peak design values. This configuration is known as a "Strong Column / Weak Connection". This failure is initiated by the inelastic deformation of one or more of the following components: anchor rods, concrete, grout, weld, or base plate. The design of all these components will have a combined effect on the CBP connection's stiffness, strength, and deformation capacity. The main purpose of this research is to perform an experimental study to investigate the behaviour of exposed CBP connections subjected to axial and bi-directional lateral loading to provide further insight into to the design of these types of connections to achieve a strong connection failure. This will be achieved through the pursuit of the following objectives: (i) experimental investigation of column base plates under combined axial load and bi-axial bending, (ii) finite element simulation of base plates under combined axial load and bi-axial bending, (iii) reliability analysis study to identify the parameters that influence the behaviour of exposed column base plates. Four large-scale CBP connection specimens have been tested to observe the effects of anchor rod pattern and base plate thickness. General purpose finite element software ABAQUS has been used to develop finite element models for reliability analysis. Experimental results are used to validate the finite element models. Different parameters such as the base plate thickness, number of anchor rods, anchor rod diameter, and

anchor rod grade are considered for the reliability analysis. The outcome of this study will aid in evaluating the influencing parameters for the design of column-base plate connections under bi-axial bending and investigating the effects of the relative strength ratio among the connection elements. It will also guide the future design of CBP connections to satisfy the combined axial load and bi-directional lateral loading conditions.

Acknowledgements

This study is based on research supported by the Canadian Institute of Steel Construction (Award no. CISC 2019-04). The support is acknowledged. Any opinions, findings, conclusions or recommendations expressed in this paper are those of the authors and do not necessarily reflect the views of sponsors. The authors also acknowledge the support provided by the laboratory personnel at the Wood Innovation Research Laboratory and Wood Innovation Design Center at the University of Northern British Columbia and Lakehead University.

I dedicate this thesis to my best friend, Gordon, and my father, Beau.

Table of Contents

List of Tables

List of Figures

Nomenclature

Symbols

A_n	Unthread portion of Anchor rod (mm^2)
B	Base Plate Length (mm)
d_c	Depth of Column (mm)
E_{col}	Elastic modulus of steel (MPa or GPa)
e_b	Distance between center of outer anchor rod to the edge of column flange (mm)
F	Lateral Force (kN)
f_c'	Concrete or Grout compressive strength (MPa)
f_u	Ultimate Strength (MPa)
f_y	Yield Strength (MPa)
H_{col}	Height of Column or Distance to Center of Lateral Actuators (mm)
I_{col}	Moment of Inertia of Column (mm^3)
M	Base Moment (kN x m)
$Mf_{,plate}$	Flexural Demand of Base Plate (kN x m)
M_{max}	Max Base Moment (kN x m)
Mp_c	Plastic Moment of Column (kN x m)
Mp_p	Plastic Moment of Base Plate (kN x m)
N	Base Plate Width (mm)
P	Axial Load (kN)
T_r	Anchor Rod Tension Resistance (kN)
T_f	Anchor Rod Tension Demand (kN)
Y	RSB Stress Block Width (mm)
θ	Base Rotation (% rad)
Δ_{top}	Lateral Displacement (mm)
Φ_{ar}	Anchor Rod Resistance Factor
Φ_{bp}	Base Plate Resistance Factor
Φ_c	Column Resistance Factor
Φ_{conc}	Concrete Resistance Factor

Abbreviations

BP	Base Plate
CBP	Column Base Plate
FBD	Free Body Diagram
FEM	Finite Element Model
MCS	Monte Carlo Simulation
RSB	Rectangular Stress Block
Bf	Column Flange Width (mm) used in MCS
BFy	Base Plate Yield Strength (MPa) used in MCS
Bg	Base plate edge distance (mm) used in MCS
Bp	Base plate length / width (mm) used in MCS
BTf	Base plate thickness (mm) used in MCS
CFy	Column Yield Strength (MPa) used in MCS
Dc	Depth of Column (mm) used in MCS
Dr	Anchor Rod diameter (mm) used in MCS
fc	Concrete compressive strength (MPa) used in MCS
RFu	Anchor Rod Ultimate Strength (MPa) used in MCS
Tf	Column Flange Thickness (mm) used in MCS
Tw	Column Web Thickness (mm) used in MCS

Chapter 1 Introduction

1.1 Background

Exposed Column Base Plate (CBP) Connections are common connections used in low to mid-rise building construction. These connections are typically composed of a steel column that is welded to a base plate and secured to a concrete foundation utilizing anchor rods to secure the base plate. These connections are responsible for transferring the forces exerted on a column into the base foundation of a structure and can have a devastating impact on a structure if improperly designed. Special attention is required when designing the anchor rods and base plate of a CBP connection to account for an uplift condition that must be resisted when lateral force(s) are applied to the top of the column. Improper design of a CBP connection will result in a weak connection which is attributed to the failure of the connection components (anchor rods, base plate, grout, etc.) before the column can reach its peak design values. Figures 1a and b depict typical exposed column base plate connection components, where Figure 1a displays one example of the connection used in the experimental study (Test 3), and Figure 1b shows the components of an exposed CBP connection.

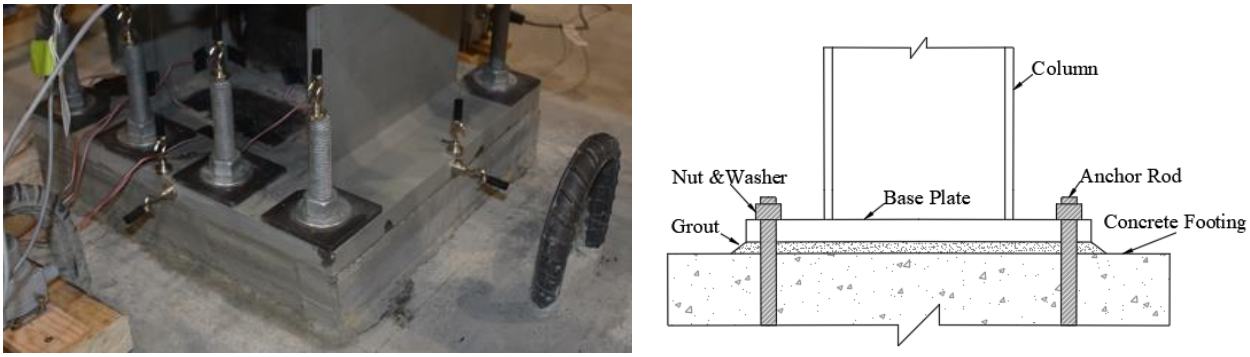

(a) *(b)*

Figure 1 Exposed CBP Connection (a) Exposed CBP Connection (Test 3) (b) Exposed CBP Components

1.2 Problem Statement

Current design codes and guidelines have limited contribution in addressing the design of exposed CBP connections under combined axial load and bi-axial bending. Although, the columns are designed and checked under combined axial load and bi-axial bending, when it comes to the base plate connection, only the axial load and major axis bending are considered. Practicing engineers often adopt complex finite element method or design them in two directions separately, which often results in overly conservative design. Thus, a more direct approach to designing CBP connections subjected to combined axial and lateral loading conditions would help ensure column base connections perform as intended under extreme loading.

1.3 Research Methodology

1. Conduct Experimental Investigation into CBP Connection Behaviour Subjected to Combined Axial and Bi-Directional Lateral Loading
2. Analyze Experimental Results and Current Design Procedures and Guidelines
3. Validate Experimental Results Using Finite Element Modeling (FEM)
4. Conduct CBP Connection Reliability Analysis using Experimental and FEM Results

1.4 Scope of Work

The main purpose of this study is to conduct an experimental investigation into CBP connection behaviour subjected to combined axial and bi-directional lateral loading. The experimental results are used to check against current design codes and guidelines to evaluate their effectiveness when subjected to bi-directional lateral loading. With the results from the experimental investigation a FEM validation is conducted which validates the results from Test 2 experimentation. With the FEM validation model further FEM models are developed which investigate varying the thickness of the base plate, anchor rod diameter, and anchor rod grade to achieve a strong connection failure. Results from the FEM models are used in a reliability analysis which classifies the failure modes for various 4-Bolt CBP connections. Through the combination of experimental and FEM results, this study classifies various CBP connections and shows the effects of varying CBP components until a strong connection failure can be achieved.

1.5 Research Objective

The main objective of this research is to provide more insight into the design of CBP connections subjected to combined axial and bi-directional lateral loading to help establish a more direct approach to designing these connections. Large-scale CBP connection testing has been conducted in this research and the experimental results have been analyzed and FEM models were generated based on the test results. With the results from the FEM models, a reliability analysis has been conducted which classifies the failure modes for various 4-Bolt CBP connection configurations. The goal of this research is to provide further insight into to the design of exposed CBP connections subjected to combined axial and bi-axial bending to achieve a strong connection failure.

1.6 Thesis Outline

This thesis is organized into seven chapters which contain the following content:

- Chapter 2 provides a detailed literature review pertaining to CBP connection design.
- Chapter 3 details the experimental program used for the CBP connection testing.
- Chapter 4 presents the results of the experimental testing.
- Chapter 5 analyzes the tests results and provides a comparison of all experimental tests.
- Chapter 6 presents a FEM validation and CBP Connection Reliability Analysis.
- Chapter 7 details the Conclusions and Recommendations for Future Works.

Chapter 2 Literature Review

2.1 General

Ensuring adequate seismic performance of a structure during a major seismic event is a growing concern across the world. Many buildings utilize exposed column base plate connections designed to resist forces only in the major direction, although the columns are designed for resisting bi-axial bending. Some of these connections may not consider the base plate uplift condition, where lateral forces are not accounted for in the base connection design. To combat this issue the SAC Joint Venture (1994) was formed to investigate damage to welded steel moment frame buildings during the 1994 Northridge earthquake. The goal of the SAC Joint Venture was to help develop new design approaches to help steel frame buildings perform more adequately when subjected to earthquakes (1994).

Previous studies have been conducted by DeWolf and Sarisley (1980) and Drake and Elkin (1999) to progress the design of base connections to account for combined axial load and moment. The American Institute of Steel Construction's Steel Design Guide-1 by Fisher and Kloiber (2006) provides a detailed design guideline for base connections commonly used for current base connection design to meet combined axial load and moment demands. Gomez (2010) further investigated the design guide one approach and extensively reviewed base connection design to meet cyclic loading only in the major direction.

Currently, there is minimal research on the design of exposed column base connections subjected to a combined axial load and bi-directional lateral loading. The difficulty lies in designing the base connection to act as a fixed connection in both the strong and weak axes. Buildings can become mechanically unstable when base plate connections are combined with pinned beam-column connections (Lim et al. 2017). This can be resolved by utilizing a fixed column base or a rigid beam-column connection to achieve stability. Both approaches can be costly and overly conservative for low to mid-rise buildings composed of low-mass sections. Choi and Choi (2013) conducted an experimental investigation on the inelastic behaviour of exposed-type steel HSS column bases under three-dimensional loadings. They concluded that the failure patterns of exposed-type column bases are significantly different under combined axial and bi-axial bending compared to uniaxial bending. Recently, Fasaee et al. (2018) conducted a numerical investigation to evaluate the capacity of flexible column-base connections under axial load and

bi-axial bending. Seco et al. (2021) investigated the response of exposed column base plates with four outer anchor bolts subjected to monotonic bi-axial bending. They concluded that the rotational stiffness and bending resistance of base connections are dependent on the direction of the applied moment. Cloete and Roth (2021) proposed a simplified theoretical model for designing column base connections subjected to axial load and bi-axial bending. However, the proposed method is conservative and does not consider the effect of loading cycles. However, there exists no study that experimentally investigated the performance of column-base connections under combined axial load and biaxial cyclic bending moment.

2.2 Base Connection Failure Categories

Fahmy (2000) presented a thorough formulation for base connection design which directly relates to three main categories of failure. The first category is Strong Column / Weak Connection failure which is initiated by the inelastic deformation of one or more of the following components: anchor rods, concrete, grout, weld, and base plate. There are six modes of failure associated with a Strong Column / Weak Connection. The first four failure modes are typically caused by an undersized base plate and are classified by the formation of yield lines along the column flanges and in between the anchor rod holes of the baseplate. The fifth mode is related to the yielding of the anchor rods (shown in Figure 2a). This occurs mainly when the anchor rods are undersized and the base plate is oversized. This mode exhibits a pinched hysteresis response caused by cumulative elongation of the anchor rod. The strength of the connection will also drop quickly during repeat cycles at the same drift level. The sixth mode is caused by the simultaneous yielding of both anchor rods and base plate. This occurs mainly when both the base plate and the anchor rod are undersized.

The second category of failure is a Weak Column / Strong Connection which is displayed in Figure 2b. This failure mode is defined by a plastic hinge forming in the column only. Connections that fail in this mode have high ductility with stable hysteresis loops and increased strength after yielding. This failure mode allows the column to reach its peak design values before failure. This failure category can be identified when buckling occurs in the column flanges before any other components begin to yield as shown in Figure 2b. The final category is a balanced failure where the yielding of the base connection and column occurs simultaneously as shown in Figure 2c.

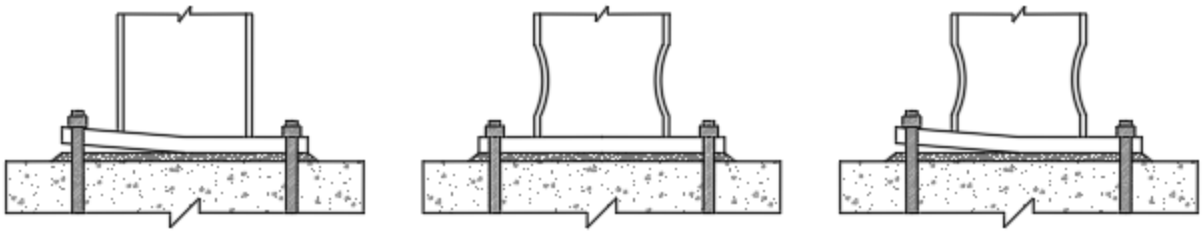

(a) *(b)* *(c)*

Figure 2 Exposed Column Base Connection Failure Categories (a) Strong Column / Weak Connection, (b) Weak Column / Strong Connection, (c) Balanced.

2.3 Current Design Procedures

2.3.1 Resistance Equations - CSA S16-14

CSA S16-14 (2016) provides resistance equations for all the steel components used in base connection design. Equation 1 displays how to compute the plastic moment in the column in the major direction, where Equation 2 indicates the plastic moment of the column in the minor direction. F_y refers to the yield strength of the column, where Z_x and Z_y are the plastic section modulus for the major (flange) and minor (web) axes respectively. These two resistance checks will be used to predict if the column buckles in the flange or web due to the demand of the specific test. Equation 3 calculates the tension force resistance in a singular rod. A_n refers to the unthreaded portion of the rod, which requires a reduction of 0.85. F_u refers to the ultimate strength of the anchor rod. Equation 4 shows how to calculate the plastic moment of a base plate, where t_p is the thickness of the plate. Equation 5 provides the resistance reduction values for the column (φ_c), base plate (φ_{bp}) and anchor rod (φ_{ar}).

$$\boldsymbol{M_{px,colm} = \varphi_c \times Z_x F_y} \quad (1)$$

$$\boldsymbol{M_{py,colm} = \varphi_c \times Z_y F_y} \quad (2)$$

$$\boldsymbol{T_{r,rod} = \varphi_{ar} \times A_n \times F_u} \quad (3)$$

$$\boldsymbol{M_{p,plate} = \varphi_{bp} \times Z_y F_y = \varphi_{bp} \times \frac{F_y \times t_p^2}{4}} \quad (4)$$

$$\boldsymbol{\varphi_c = \varphi_{bp} = 0.9,\ \varphi_{ar} = 0.67} \quad (5)$$

2.3.2 Connection Strength Ratio

The three categories of CBP connection failure are further characterized by a plastic moment ratio (Γ) shown in Equation 6. This is a ratio between the column plastic moment ($Mp_{c)}$ and the sum of the moment capacities of the base connection components. The symbol d_c refers to the depth of the column, where e_b is the distance from the center of the outer anchor rod to the edge of the column flange. The ratio is derived from a plastic analysis of the connection which considers two plastic moments forming in the base plate at the edge of the column flanges (Mp_p). The tension force demand (T) for the anchor rod to resist baseplate uplift is shown in Equation 7. Equation 8 combines Equations 1 and 2 to make a simplified equation for the Connection Strength Ratio. If the ratio is greater than 1 the failure mode is anticipated to be a Strong Column / Weak Connection. If the ratio is less than 1 the failure mode is a Weak Column / Strong connection. If the ratio is equal to 1 then the failure mode is balanced. Equation 9 displays the reduction required to the rod resistance when additional rods are located within the depth of the column (8-Bolt Parallel Configuration). Figure 3 can be used to derive Equations 6 - 9.

$$\mathbf{\Gamma} = \frac{\mathbf{Mp_c}}{\underset{\mathbf{Rods}}{\overset{\mathbf{Plate}}{\mathbf{\Sigma M}}}} = \frac{\mathbf{Mp_c}}{(\mathbf{2Mp_p + Td_c})} \tag{6}$$

$$\mathbf{T} = \frac{\mathbf{Mp_p}}{\mathbf{e_b}} \tag{7}$$

$$\mathbf{\Gamma} = \frac{\mathbf{Mp_c}}{\mathbf{Mp_p}(2+\frac{\mathbf{d_c}}{\mathbf{e_b}})} \tag{8}$$

$$\mathbf{Parallel\ Inner\ Rod\ Reduction} = \mathbf{1} - \frac{\mathbf{dist.btw\ rods} - \boldsymbol{e_b}}{\mathbf{d}_{\boldsymbol{c}}} \tag{9}$$

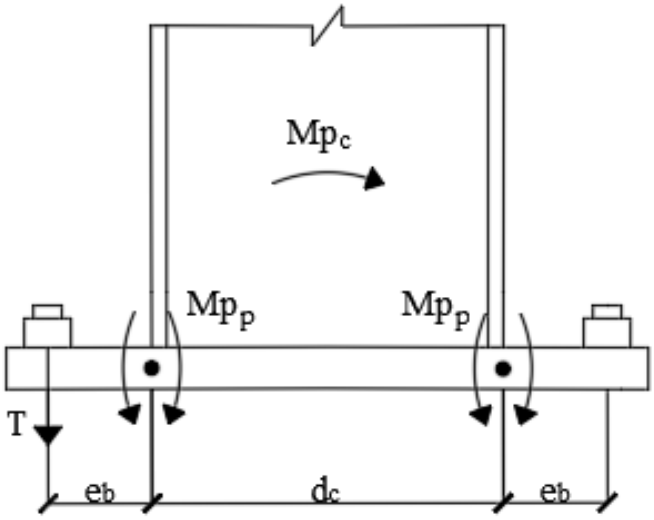

Figure 3 Connection Strength Ratio Free Body Diagram (FBD)

2.3.3 Rectangular Stress Block Method

Gomez (2010) presented a detailed guide on column base plate design which follows the design guide one approach to meet combined axial force and uniaxial moment. Rectangular Stress Block Method is displayed in Equations 10, 11, and 12, where only the uplift condition is considered. The values (B and N) shown in Equations (10-12) are the length and width of the base plate, respectively, which are the same (square plate) for all tests, and the value (g) is the edge distance of the baseplate to the center of the rods. Using Figure 4 FBD by method of force equilibrium, the Axial Force (P) and Moment (M) can be computed as shown in Equations 10 and 11, respectively. Equations 10 and 11 can then be solved simultaneously for the tension force demand in the anchor rod (T), as shown in Equation 12. Equation 13 shows how to calculate the f_{max} used in Equation 12. Φ_{conc} is a reduction factor of 0.65 provided by CSA A23,3-14 (2016). Equation 14 shows the equation provided in clause 10.8 of CSA A23.3-14 for calculating the concrete bearing stress. Equation 15 displays the how to calculate the flexural demand in the base plate based on the tension force demand obtained from the Design Guide One Approach. Equation 16 indicates how to calculate the lever arm for the flexural demand in the base plate.

$$\mathbf{P} = (\mathbf{f_{max}} \times \mathbf{Y} \times \mathbf{B}) - \mathbf{T} \tag{10}$$

$$\mathbf{M} = (\mathbf{f_{max}} \times \mathbf{Y} \times \mathbf{B})\left(\frac{\mathbf{N}}{2} - \frac{\mathbf{Y}}{2}\right) + \mathbf{T}\left(\frac{\mathbf{N}}{2} - \mathbf{g}\right) \tag{11}$$

$$\mathbf{T} = \mathbf{f_{max}} \times \mathbf{B}\left[(\mathbf{N} - \mathbf{g}) - \sqrt{(\mathbf{N} - \mathbf{g})^2 - \frac{2[\mathbf{M} + \mathbf{P}\left(\frac{\mathbf{N}}{2} - \mathbf{g}\right)]}{\mathbf{f_{max}} \times \mathbf{B}}}\right] - \mathbf{P} \tag{12}$$

$$f_{max} = min[f_c' \, grout, \; Conc. Bearing \; Stress] \times \varphi_{conc} \tag{13}$$

$$f_{conc\ bearing} = 0.85 \times f_c' \times \sqrt{\frac{A_2}{A_1}} \leq 1.7 \times f_c' \tag{14}$$

$$M_{f,plate} = \frac{T_f \times Y_{arm}}{Base\ Plate\ Length} \tag{15}$$

$$Y_{arm} = \frac{Length\ of\ Plate}{2} - g - (0.475 \times Depth\ of\ Colm) \tag{16}$$

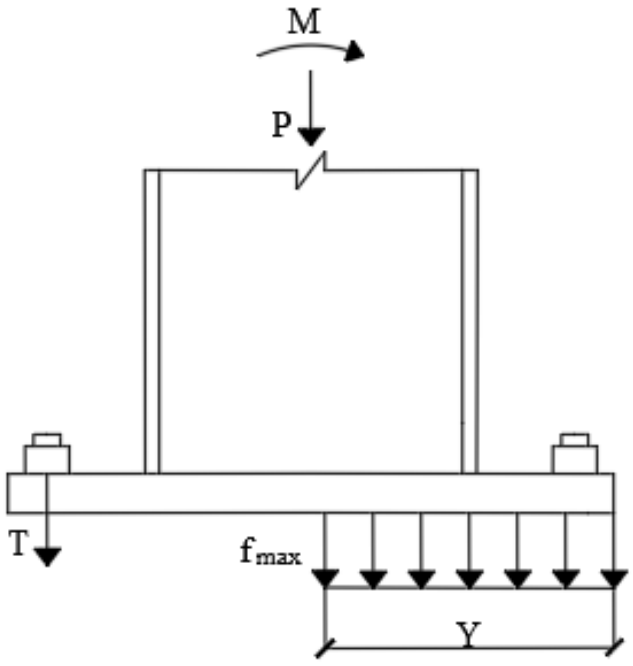

Figure 4 Design Guide One – Rectangular Stress Block Method FBD

2.3.4 Column Base Rigidity

Column-base connection is typically considered as either rigid or pinned during design consideration (Borzouie 2016). Eurocode 3 (EN 1993) classifies base connection rigidity into three classes such as rigid, semi-rigid, and pinned depending on the different base rotational stiffness (K_θ) limit expressed by Equations 18, 19 and 20, respectively. As shown in Equation 17, the base rotational stiffness can be calculated by dividing the base moment (M) by the base rotation (θ). Column base connections having base rotational stiffness of 30(EI/H) or greater are considered as fully rigid whereas it is considered as fully pinned when the base rotational stiffness is less than 0.5(EI/H). Base connections with rotational stiffness between these two limits are considered to be semi-rigid.

$$\boldsymbol{K_\theta = \frac{M}{\theta}} \tag{17}$$

$$\boldsymbol{K_\theta \geq 30\,(\frac{EI}{H})_{col}} \tag{18}$$

$$\boldsymbol{0.5(\frac{EI}{H})_{col} < K_\theta < 30(\frac{EI}{H})_{col}} \tag{19}$$

$$\boldsymbol{K_\theta < 0.5(\frac{EI}{H})_{col}} \tag{20}$$

2.4 CBP Connection Reliability Analysis

2.4.1 Background

Currently, there is minimal research pertaining to the reliability analysis of exposed column base connections subjected to a combined axial and bi-directional lateral loading using current design procedures (Design Guide One). Safety evaluation of CBP connections is a paramount duty, which is dependent on various failure modes. The typical safety of a structure depends on the resistance of the member and the load applied. Manjunath (2015) explains how a structure's resistance depends on its members' geometric and physical properties, which can be considered probabilistic in nature (2015). Song (2021) explains how reliability analysis using Monte Carlo Simulation may define the uncertainties in the loads, material properties/geometry, and demand and capacity for the specific connection elements.

Song (2021) conducted an extensive CBP reliability analysis study based on Monte Carlo Simulation using Design Guide One Approach. Some critical conclusions were found and implemented into the Monte Carlo Simulations utilized in his study. Songs findings are listed below;

1. Flexural yielding of the baseplate on the compression side does not fail unless combined with yielding of the anchor rods or by yielding of the baseplate on the tension side. This, in turn, means one only needs to design the tension side of the base plate.

2. Applying design checks independently is inappropriate because failing one design check may only partially lead to the connection's failure.

3. The bearing stress in the concrete includes a resistance factor that incorporates the uncertainty of stress. This factor is not suitable for the design of the base plate and anchor rods.

4. The resistance factors used in the design checks for the anchors and baseplate are not based on reliability analysis. The checks only consider the uncertainty in the capacities of the components, where the uncertainty in the estimated forces and moments within these components is disregarded.

Chapter 3 Experimental Program

3.1 Test Matrix and Description

The test matrix shown in Table 1 displays the differences between the four experiments. Tests 1 and 2 use 4-Bolt anchor rod patterns, whereas Tests 3 and 4 use 8-Bolt (parallel) patterns. Tests 1 and 3 use 25mm thick baseplates, whereas Tests 2 and 4 use 38mm thick baseplates. The base plate thicknesses were varied to observe the effects of using a thinner base plate and to compare yielding of the component. The grout height was changed to account for the change in baseplate thickness; this was required so the actuator connection would align properly for all experiments. The baseplate hole patterns for Test 1 and 2 (4-Bolt) and Test 3 and 4 (8-Bolt) are displayed in Figure 5.

Table 1 Test Matrix

Test #	BP Dimensions (mm)	Bolt Pattern	Axial Load (kN)	Lateral Loading	Grout Height (mm)
1	407x407x25	4	400	Bi-Directional	64
2	407x407x38	4	400	Bi-Directional	51
3	407x407x25	8	400	Bi-Directional	64
4	407x407x38	8	400	Bi-Directional	51

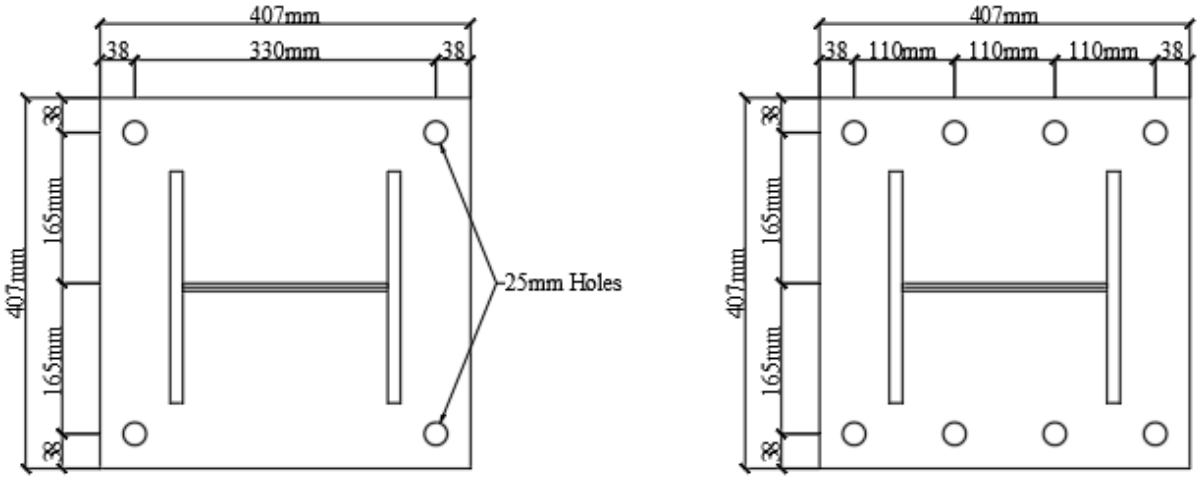

(a) *(b)*

Figure 5 Base Plate Configuration: (a) 4-Bolt Configuration (Test 1 and 2), (b) 8-Bolt Configuration (Test 3 and 4)

The column section is considered as W250x73 which reflects the typical members that are used as first-story interior columns of steel moment frames in low to high-rise steel buildings in high seismic regions (Elkady and Lignos 2014). The length of the column is considered as 1500 mm from the top of the base plate that represents a half-scale column. Four steel wide flange columns (W-section) are considered that are welded to the center of the base plate. The column sections are designed according to the requirements of CSA S16-14 and conform to ASTM A992 Grade 50. All the columns are designed considering yield strength (F_y) of 345 MPa and modulus of elasticity of 200 GPa. The cross sections are selected to prevent local buckling criteria as well as its capacity to ensure its effectiveness before the failure of the base connection. A square base plate (407 mm x 407 mm) of Grade 300W steel with two different thicknesses of 25 mm and 38 mm is selected for column base connection. The dimensions of the baseplate were designed so the column could fit properly with enough room for bolt holes along the edges. 12mm fillet welds were used to attach the perimeter of the column base to the baseplate. SAE J429 anchor rods of 20 mm diameter are selected. Anchor rods are designed following the requirements of CSA S16-14 and CSA A23.3-14 to prevent any type of failure in the concrete by pullout or breakout strength. The nut and washers are selected according to standard geometry for the specific anchor rod. High-strength non-shrink grout is considered between the pedestal and the base plate. The grout was designed to be at least twice the compressive strength of the concrete. A 1524x1524x460 mm concrete footing is considered for the foundation of the column base connection. Table 2 depicts the material properties of the components used in the experiments. The base plate and column material properties were obtained from material testing reports provided by the steel manufacturer.

Table 2 Material Properties

Component	Modulus of Elasticity (GPa)	Yield Strength (MPa)	Ultimate Strength (MPa)
W250x73 Column	200	390	524
Base Plate (25mm)	200	366	513
Base Plate (38mm)	200	363	533
Anchor Rod	200	364	427
Concrete	-	-	32*
Grout	-	-	75*

* *notates the Compressive Strength (f_c') for Concrete and Grout*

3.2 Test Preparation

The initial process began with constructing the concrete pedestal forms (footings) and preparing the rebar cages for each test. 15M bars were used for all the longitudinal bars and stirrup cages. 25M bars were used for the center cage U-bar reinforcement, and hoops. The footing design was adopted from the Gomez (2010) experiments, where a similar configuration was used. Uniaxial strain gauges were attached to all anchor rods and all wires were run through conduit to the exterior of the footing. Resistances in the gauges were checked before and after the concrete pour. The rods were embedded 400mm (16 inches) in the concrete. The bottom (embedded) ends of the anchor rods were attached to 20mm USS washers sandwiched between two grade A hex nuts, which provided the rods with additional strength to resist pull-out. Non-shrink high strength grout was utilized between the column and baseplate and given a minimum of 28 days to cure before testing (similar to concrete). Two pedestals were poured at a time in order to re-use the form to save money. Pedestals were constructed so they could be moved from casting site to experimentation laboratory.

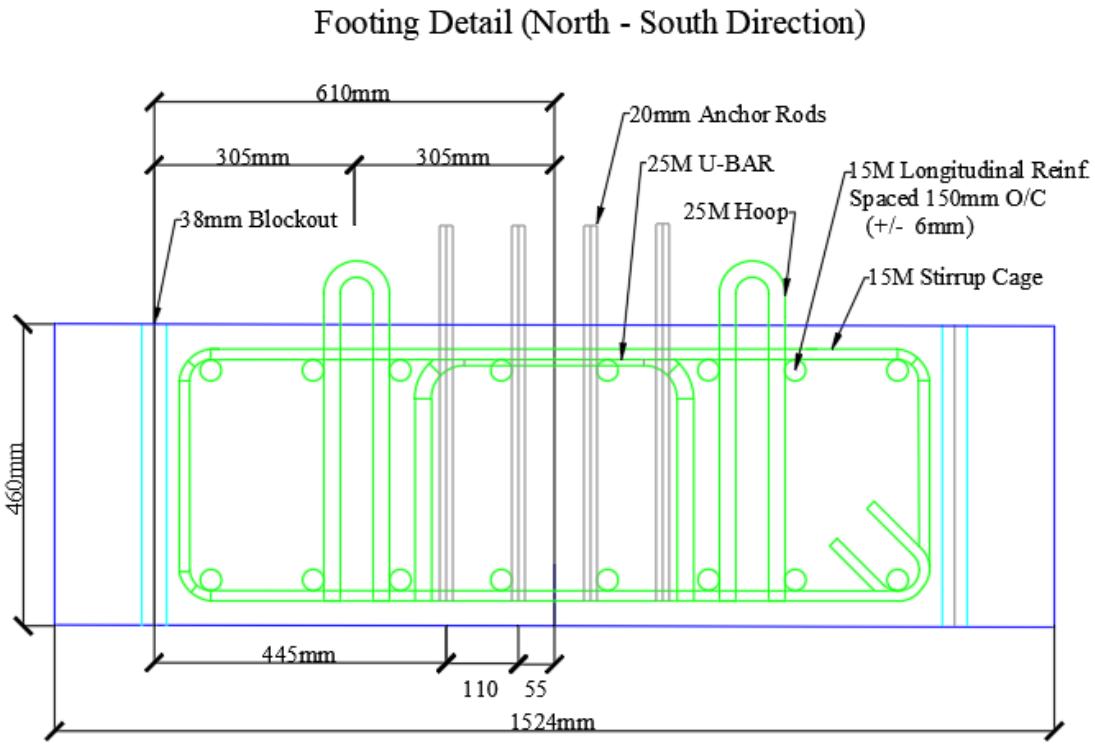

Figure 6 Concrete Pedestal Footing Detail

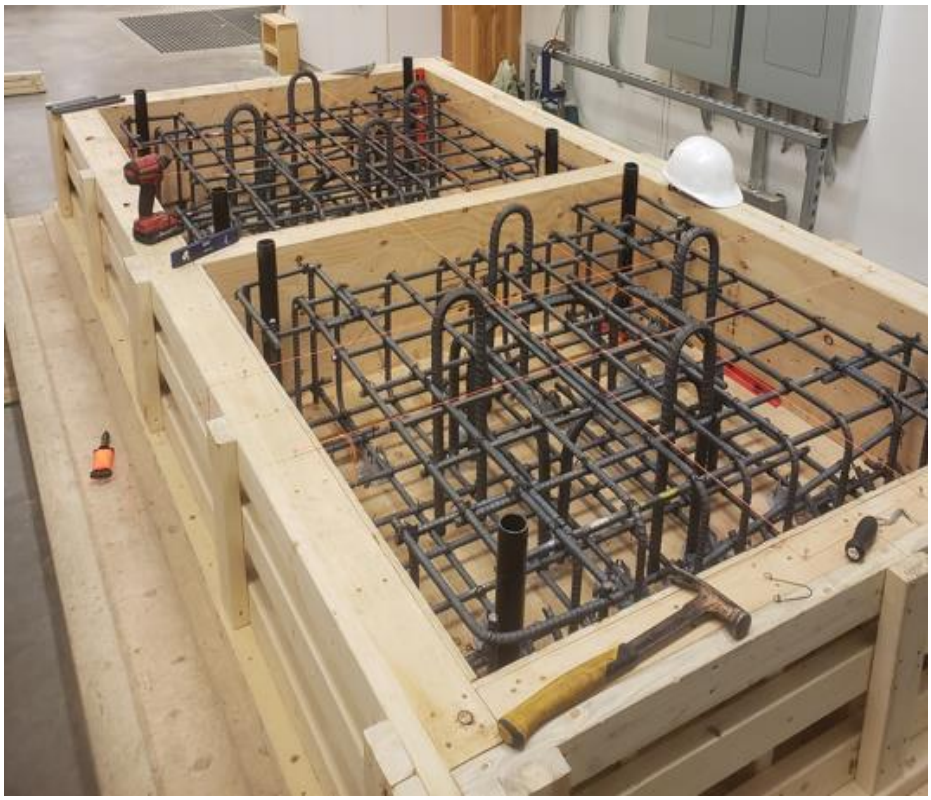

Figure 7 Concrete Pedestal Forms Before Pour

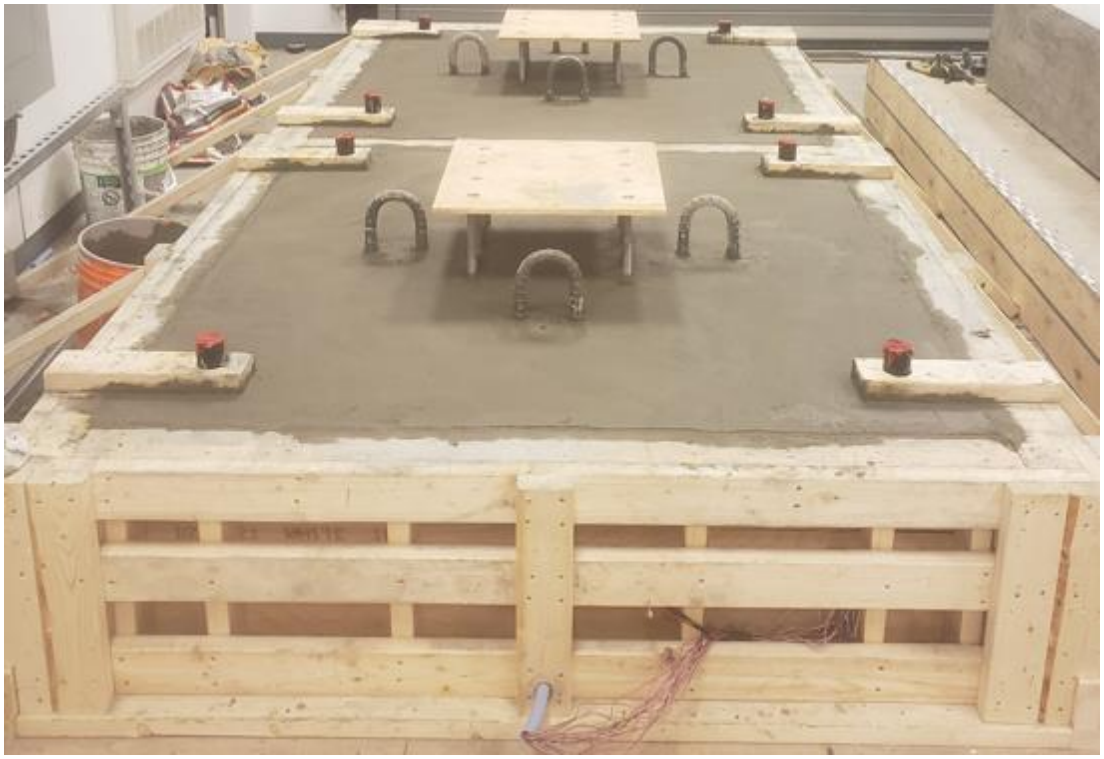

Figure 8 Concrete Pedestal Forms After Pour

3.3 Test Setup

After all concrete pedestals were prepared the actuators were setup for the experimental testing. The setup required a 250 kN actuator in the N-S direction for the minor axis loading, a 500 kN actuator in the E-W direction for the major axis loading, and a 500 kN actuator for the vertical axial force in order to apply the bi-directional lateral loading protocol. Figures 9 - 11 show the setup used for all the tests. Four tall columns were set into place after the lateral actuators were bolted to the walls. The columns carry the bridge, which bears a 38mm plate connection to the 500 kN vertical actuator. This vertical actuator provides the axial load for all the specimens. The concrete pedestals were fastened to the lab strong floor at four points at 1220mm (4‘) on center with 28mm dia. rods and 150mm square plates (12mm thick) to prevent the footing from slippage or uplift. Grade A hex nuts, USS 20mm washers, and 75mm square plate washers (6mm thick) were used to secure the 20mm SAE J429 Grade 2 anchors rods to the base plate. After all final adjustments were made with actuators, the hex nuts were tightened to snug tight plus a ¼ turn. Before testing; the W250x 73 columns were checked for plumb in both directions, safety chains were loosened on all actuators, and hydraulic lines and wires were checked.

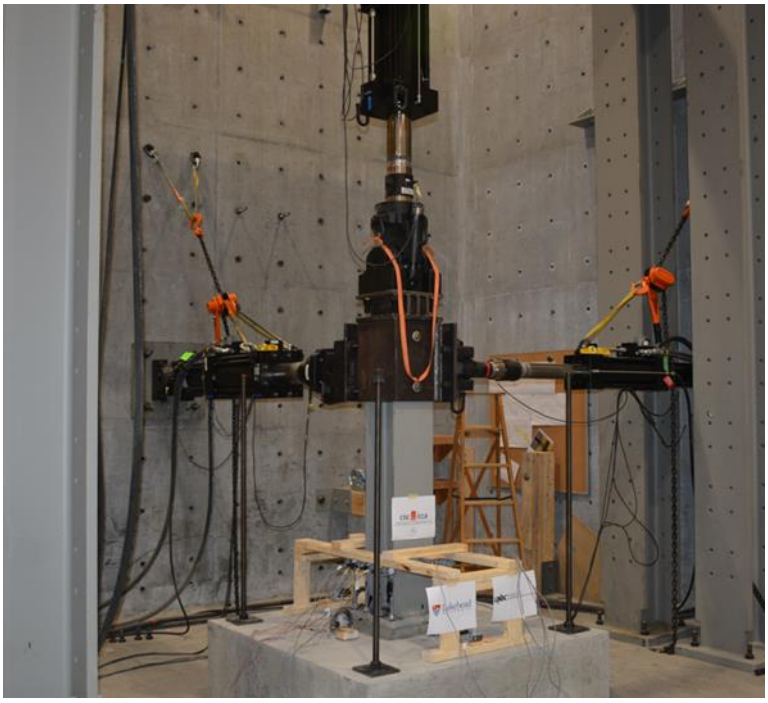

Figure 9 Test Setup

Figure 10 Bridge for Vertical Actuator Connection

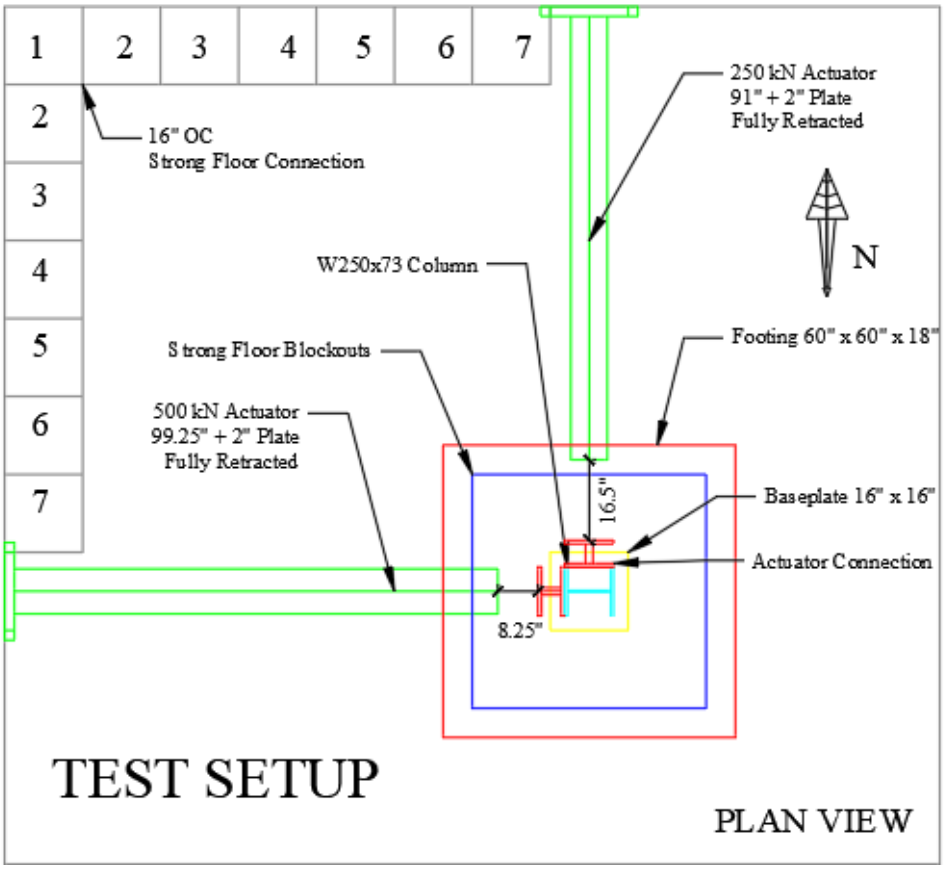

Figure 11 Test Setup Details

3.4 Actuator Connection

A special connection was required to tie in all the actuators to the W250 x 73 column. Figure 12 depicts the detail engineered to apply the three directional loadings to the column. The connection was designed to be strong enough to withstand the testing from all four experiments and to adequately distribute the forces from the major and minor lateral actuators through the flange and web of the column, respectively. The connection is a built-up section composed of a rectangular HS section that wraps around the column and is welded to separate beam sections which are attached to the actuators. The inside of the connection has welded components to allow adequate transfer of the minor lateral forces to the web of the column. Setting screws were tapped into the section to allow for additional connectivity between the connection and the column. After the connection is fitted to the column the total height from the top of the baseplate to the centerline of the lateral actuators is 1280mm.

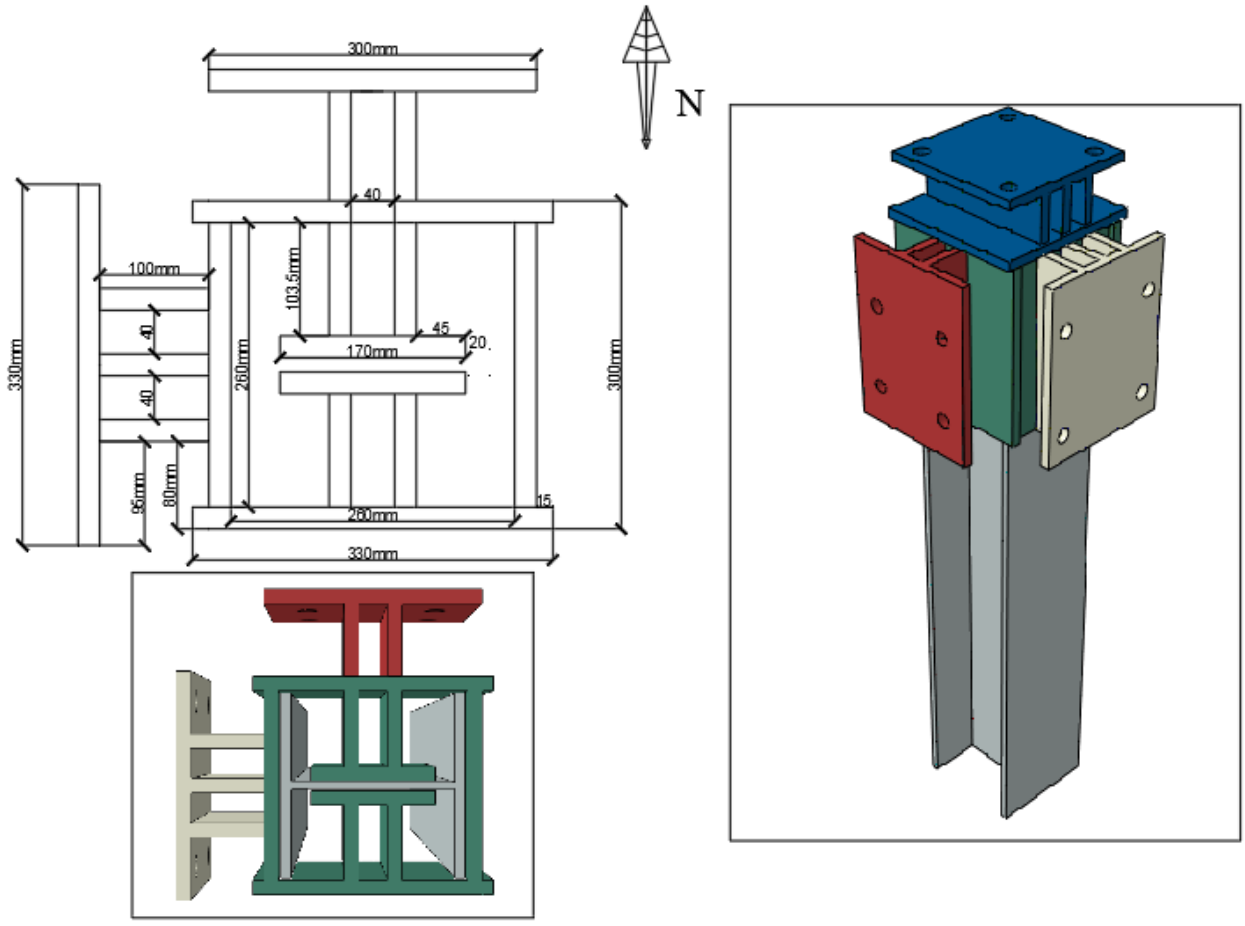

Figure 12 Actuator Connection Details

3.5 Instrumentation

A total of 30 sensors were used for Test 1 and 2 (14 string potentiometers and 16 strain gauges). Test 3 and 4 used 40 sensors total (16 string potentiometers and 24 strain gauges). String potentiometers were setup to capture the uplifts and lateral slips of the base plate for both E-W (Major) and N-S (Minor) directions. The elongations of all anchor rods were captured using string potentiometers. The forces and lateral displacements produced by the actuators were recorded directly through the actuators using MTS software. Figures 13 - 14 show the instrumentation setup for the 4-Bolt and 8-bolt tests. Strain gauges were attached to 4 positions on the column and baseplate to capture vertical and horizontal strain. Two uniaxial strain gauges (120 ohm) were attached to every anchor rod (Figures 14 and 15) approximately 60mm below the surface of the concrete. All strain gauges were run through a set of Vishay 8000 systems and data was recorded using strain smart software.

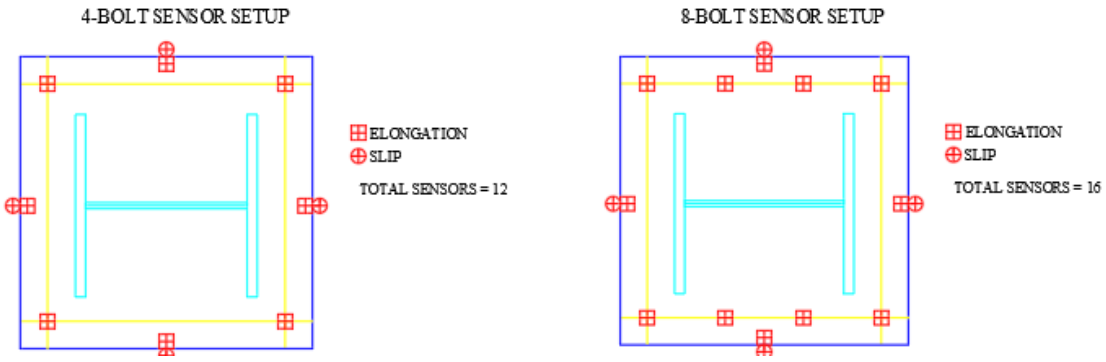

Figure 13 Instrumentation: String Potentiometer Setup

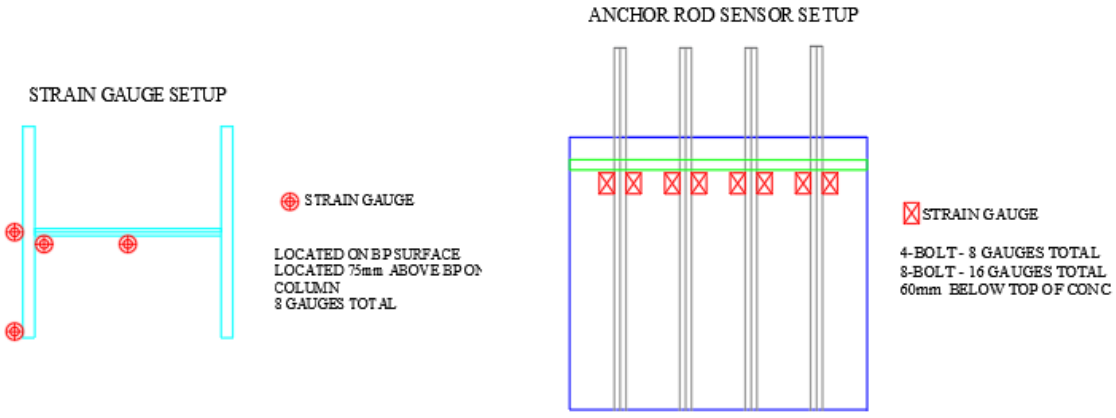

Figure 14 Instrumentation: Strain Gauge Setup

Figure 15 Anchor Rod Strain Gauge Assembly

3.6 Loading Protocol

An elliptical bi-directional lateral loading protocol (Figure 16b) was developed for the experiments. The elliptical protocol was derived from the SAC cyclic loading protocol shown in Figure 16a. The SAC cyclic loading protocol was used in the Gomez (2010) experiments and a modified version was used in the Fahmy (1999) experiments. The shape of the elliptical is based on the major lateral drift being twice the size of the minor lateral drift for each cycle. For instance during the 1.5% major lateral drift cycle the minor drift would reach a max of 0.75% minor lateral drift. Major refers to the E-W direction where the 500 kN actuator attaches to the flange of the column. Minor refers to the N-S direction, where the 250 kN actuator connects to the web of the column. All four tests use the same loading protocol.

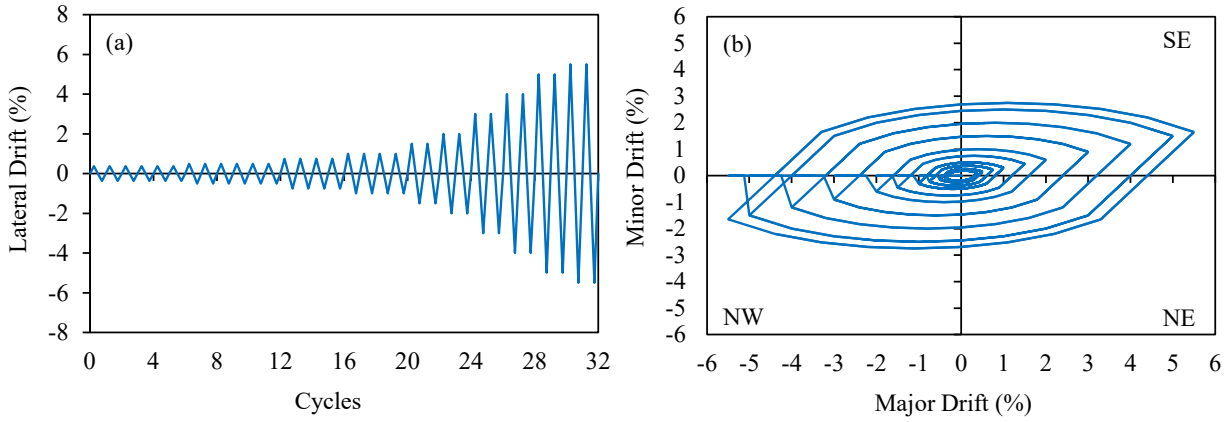

Figure 16 Loading Protocol: (a) SAC Cyclic Lateral Loading Protocol (b) Bi-Directional Elliptical Lateral Loading Protocol

The major axis displacement displayed in Figure 17a follows the specified lateral drift cycles of the SAC cyclic loading protocol shown in Figure 16a. The lateral drift was applied to the protocol as a displacement by multiplying the drift percentage by 1.28m (the distance to the centerline of the lateral actuators). There was a modification made to account for transitioning to new cycles which was needed to maintain a bi-directional lateral loading the actuators could follow. The cycles were adapted to run within a 1.5-hour time frame. The early major drift cycles which were under 1%, were shortened to run quicker at the beginning of the tests. The cycles after 1% were stretched to account for a quasi- static loading condition.

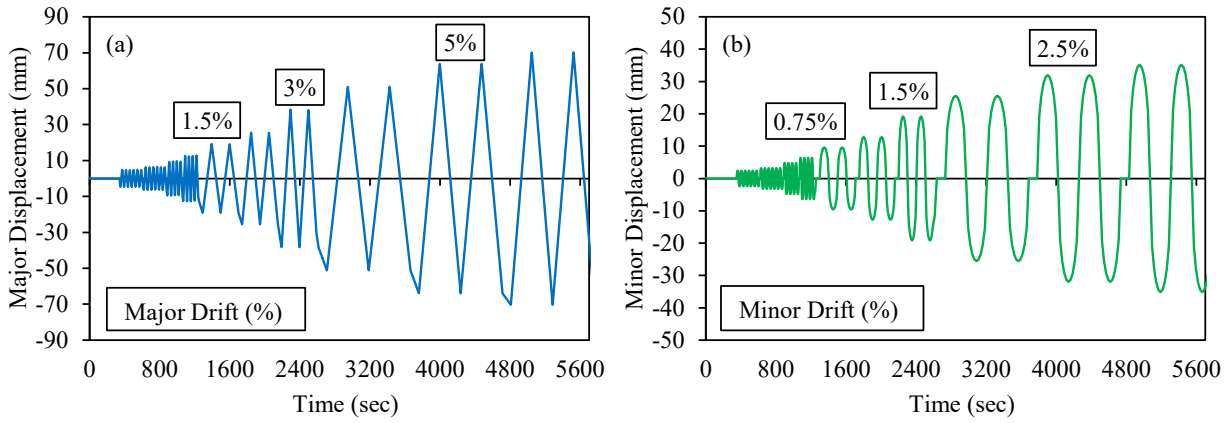

Figure 17 Loading Protocol: (a) Major Displacement vs. Time, (b) Minor Displacement vs. Time.

The minor axis displacement displayed in Figure 17b was developed to form an elliptical motion when applied simultaneously with the major axis displacement. The axial force actuator was programmed to ramp a force of 400 kN over the first 5 minutes (300 sec) of each test. Once the 400 kN is reached the vertical actuator is programmed to keep a constant 400 kN axial load on the specimen until the end of testing. It was decided to stop the tests after 5.5% major lateral drift. Major lateral displacement maxed out at 70mm (E-W direction). Minor lateral displacement maxed out at 35mm (N-S direction).

Chapter 4 Test Results

4.1 Background

This chapter presents the results obtained from the four CBP connection experimental tests. Figure 18 displays the parameters associated with CBP behaviour which were captured during experimentation. Base moment versus base rotation for both major and minor directions are plotted to show the hysteric response of each test. Equation 21 shows how to calculate the base moment, where the major/minor lateral force (F) is multiplied by the column height or in our case the distance to the center of the lateral actuators which is 1280mm. Equation 22 displays the calculation for the base rotation. All four tests were found to be weak connections where base plate uplift is engaged and the rods reached their yield point. Base moment versus base plate uplift graphs is presented for each test to show when the uplift is engaged and how it affects the moment capacity of each specimen. The uplift graphs also display the amount of crushing that is experienced at the edges of the grout. Anchor rod axial force and elongation results are displayed for each test which clearly shows when the yielding of the rods occurs in each test.

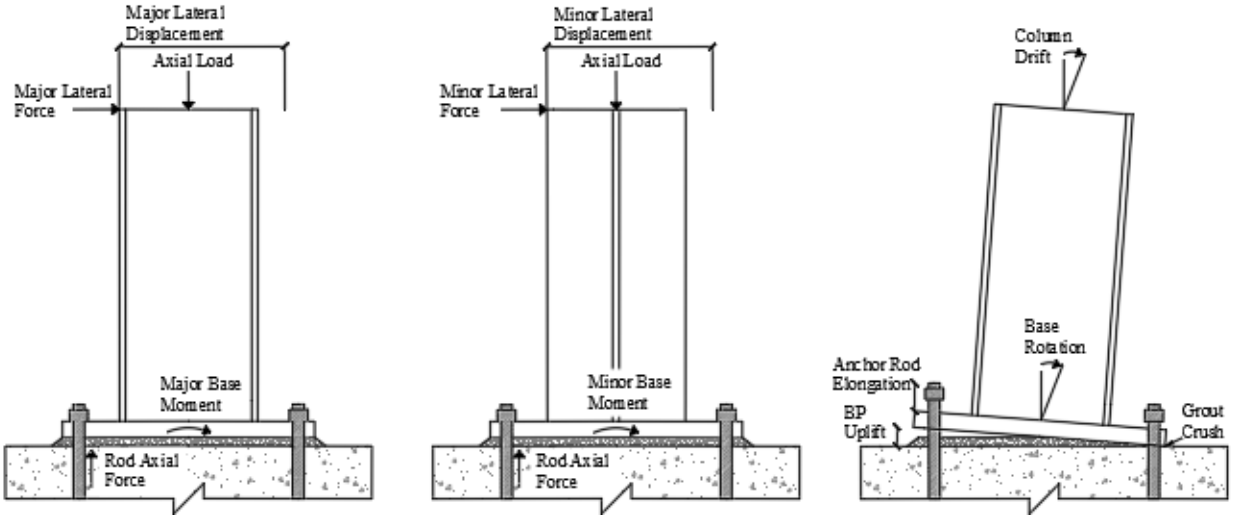

Figure 18 CBP Connection Parameters

$$\mathbf{M} = \mathbf{F} \times \boldsymbol{H_{Col}} \tag{21}$$

$$\boldsymbol{\theta} = [\Delta_{top} - \frac{\mathbf{F} \times \boldsymbol{H_{Col}}^3}{3\boldsymbol{E_{Col}}\boldsymbol{I_{Col}}}] \times \frac{\mathbf{1}}{\boldsymbol{H_{Col}}} \tag{22}$$

4.2 Test 1 – 4-Bolt Configuration (25mm BP)

Figure 19a depicts the base moment generated by the major lateral force in relation to the major base rotation. A maximum base moment of -94.7 kN x m was experienced during the first 1% drift pull cycle in the western direction (-1% rad). At the first 1.5% drift cycle a base moment of -89 kN x m was computed. In the eastern direction a maximum moment of 91.8 kN x m occurred during the first 1.5% push drift cycle. Figure 19a shows how the test specimen begins to fail after the first 1.5% drift cycle in the eastern direction and after the first 1% drift cycle in the western direction.

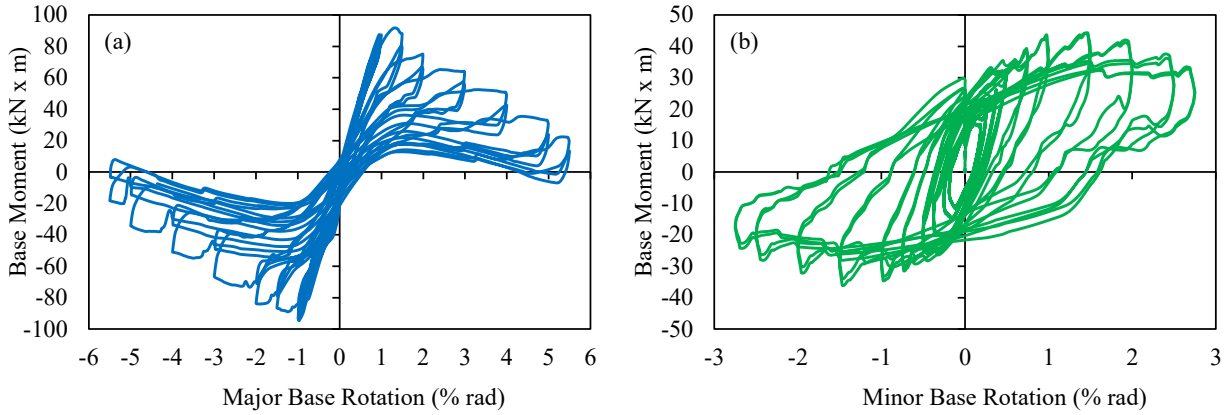

Figure 19 Test 1 Results (a) Major Base Moment vs. Base Rotation (b) Minor Base Moment vs. Base Rotation

Figure 19b depicts the base moment generated by the minor lateral force in relation to the minor base rotation. A maximum base moment of 44.2 kN x m occurred during the first 1.5% drift push cycle in the southern direction. During the first 1% minor drift cycle a base moment of 43.5 kN x m was recorded. In the northern direction a maximum moment of 36.2 kN x m occurred during the first 1.5% minor pull drift cycle. It is clear from Figure 16b that the test specimen begins to lose its ability to resist the forces acting in the minor direction during the first 1.5% drift cycle in both the southern and northern direction.

Figure 20a depicts a graphical representation of Major Base Moment versus Base Plate Uplift (East). The maximum uplift occurs at the 5.5% major lateral drift cycle (5.5% rad) for both sides of the baseplate. The maximum uplifts are 14.8mm on the east side of the base plate and 14 mm on the west. The uplift is noted to be less than 3mm for the initial major drift cycles up until the

start of the 1.5% lateral drift cycle. After 1.5% major lateral drift the uplift begins to increase more rapidly similar to the lateral displacement.

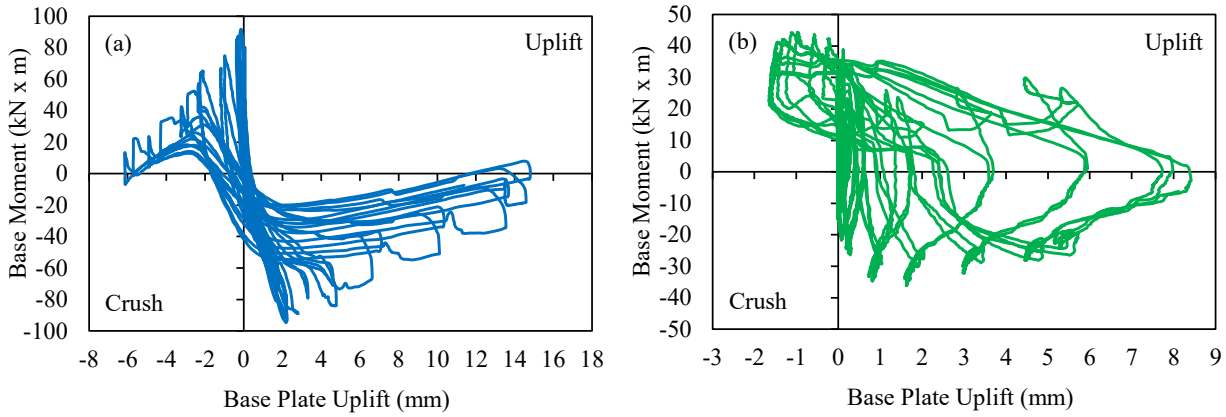

Figure 20 Test 1 Results: (a) Major Base Moment vs. Base Plate Uplift (East) (b) Minor Base Moment vs. Base Plate Uplift (South)

Figure 20b displays Minor Base Moment versus Base Plate Uplift (South). The maximum minor uplift occurs during the 2.75% minor lateral drift cycle for the north and south sides of the base plate. The maximum uplifts are 8.4mm for the south side and 7.5mm for the north side of the baseplate. The uplift is less than 2.5mm for the initial drift cycles up until the end of the 1% lateral drift cycle. After 1% drift the uplift doubles the previous 1% values at the 1.5% drift cycle.

Figure 21a depicts the axial force for the NW anchor rod recorded throughout the test. Figure 21b displays the elongation results for the SE anchor rod. The NW rod was the first rod to yield during the experiments. The SE anchor rod experienced the greatest elongation out of all the rods. It is shown in Figure 18a that the NW rod is engaged elastically at 0.5% major lateral drift. The NW and SE rods begin to take on more force and stretch at an increased rate at 1% major lateral drift. The NW rod yields during the first 1.5% major lateral drift cycle at a peak force of 110.25 kN. Rod force results were computed by converting strain gauge readings based on the rod material properties acquired from laboratory tension testing. The axial force results show how the force does not drop back to zero during the plastic phase which allows for easy identification of the yield point. The results recorded show that the test experienced failure due to anchor rod yielding which categorizes the failure as a Weak Connection / Strong Column. Figure

22a displays the NW anchor rod during the 1.5% major lateral drift, where Figure 22b shows the test during the final cycle at 5.5% major lateral drift.

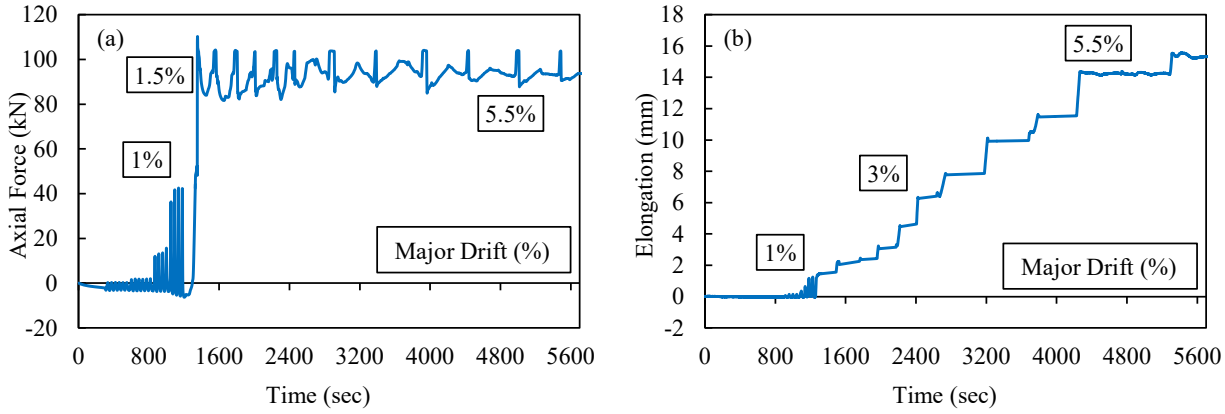

Figure 21 Test 1 Anchor Rod Results: (a) NW Anchor Rod Axial Force vs. Time (b) SE Anchor Rod Elongation vs. Time

(a) *(b)*

Figure 22 Test 1 Results: (a) Test 1 – 1.5% Drift (Rod Yield) (b) Test 2 - 5.5% Drift (Last Cycle)

4.3 Test 2 – 4-Bolt Configuration (38mm BP)

Figure 23a depicts the base moment generated by the major lateral force in relation to the major base rotation. A maximum base moment of -116.7 kN x m was experienced during the first 2% drift pull cycle in the western direction (-2% rad). At the first 1.5% drift cycle a base moment of -115.9 kN x m was computed. In the eastern direction a maximum moment of 107.1 kN x m occurred during the first 1% push drift cycle. Figure 23a shows how the test specimen begins to fail after the first 1% drift cycle in the eastern direction and after the first 2% drift cycle in the western direction.

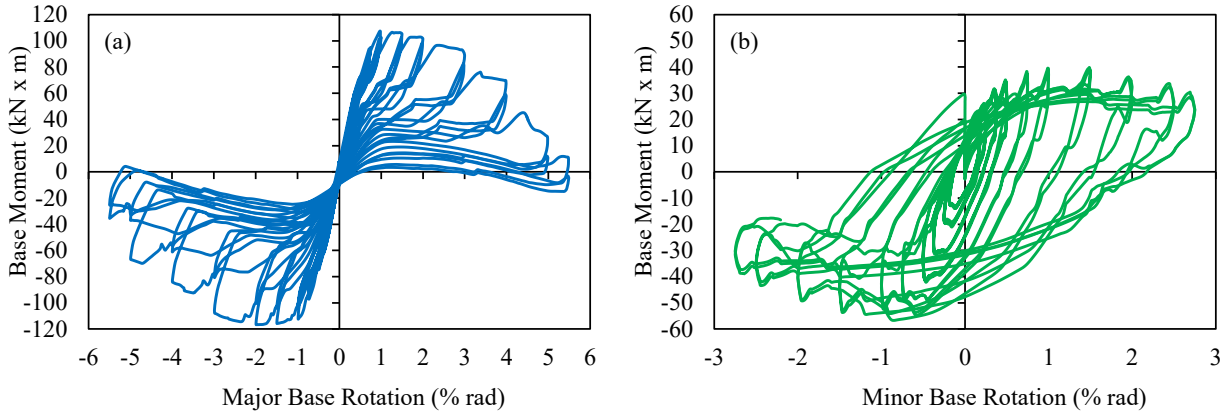

Figure 23 Test 2 Results (a) Major Base Moment vs. Base Rotation (b) Minor Base Moment vs. Base Rotation

Figure 23b depicts the base moment generated by the minor lateral force in relation to the minor base rotation. A maximum base moment of -56.7 kN x m occurred during the first 1.5% drift pull cycle in the northern direction with a corresponding base rotation of -0.87 % rad. During the first 1% minor drift cycle a base moment of -54.9 kN x m was recorded. In the southern direction a maximum moment of 40 kN x m occurred during the first 1.5% minor push drift cycle. It is clear from Figure 23b that the test specimen begins to lose its ability to resist the forces acting in the minor direction during the first 1.5% drift cycle in the southern direction and during the first 1.5% drift cycle in the northern direction.

Figure 24a depicts a graphical representation of Major Base Moment versus Base Plate Uplift (East). The maximum uplift occurs at the 5.5% major lateral drift cycle (5.5% rad) for both sides of the baseplate. The maximum uplifts are 15.8mm on the east side of the base plate and 14.9mm on the west. The uplift is noted to be less than 3mm for the initial major drift cycles up until the end of the 1.5% lateral drift cycle. After 1.5% major lateral drift the uplift begins to increase more rapidly similar to the lateral displacement.

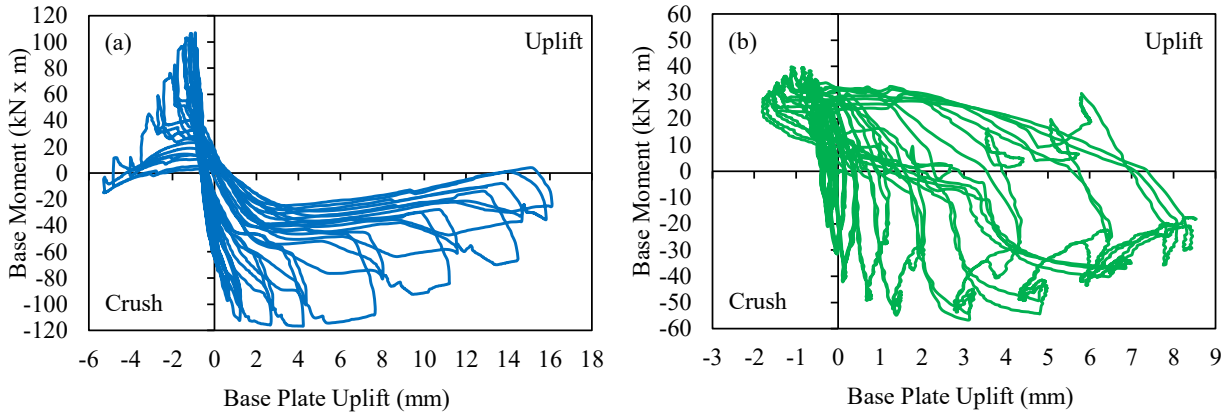

Figure 24 Test 2 Results: (a) Major Base Moment vs. Base Plate Uplift (East) (b) Minor Base Moment vs. Base Plate Uplift (South)

Figure 24b displays Minor Base Moment versus Base Plate Uplift (South). The maximum minor uplift occurs during the 2.75% minor lateral drift cycle for the south side and 2.5% for the north sides of the base plate. The maximum uplifts are 8.5mm for the south side and 7.7mm for the north side of the baseplate. The uplift is less than 2.5mm for the initial drift cycles up until the end of the 1% lateral drift cycle. After 1% drift the uplift doubles the previous 1% values at the 1.5% drift cycle.

Figure 25a depicts the axial force for the SE anchor rod recorded throughout the test. The SE rod was the first rod to yield during the experiments and was also the rod which experienced the greatest elongation. It is shown in Figures 25a and 25b that the SE rod is engaged elastically at 0.5% major lateral drift. The rod begins to take on more force and begins to stretch at an increased rate after 1% major lateral drift. The SE rod yields during the first 3% major lateral drift cycle at a peak force of 109.85 kN. At 3% drift it is clear from both Figures 25a and 25b that the rod enters its plastic phase. The results recorded show that the test experienced failure due to anchor rod yielding which categorizes the failure as a Weak Connection / Strong Column.

Figure 26a displays the SE anchor rod during the 3% major lateral drift, where Figure 26b shows the test during the final cycle at 5.5% major lateral drift.

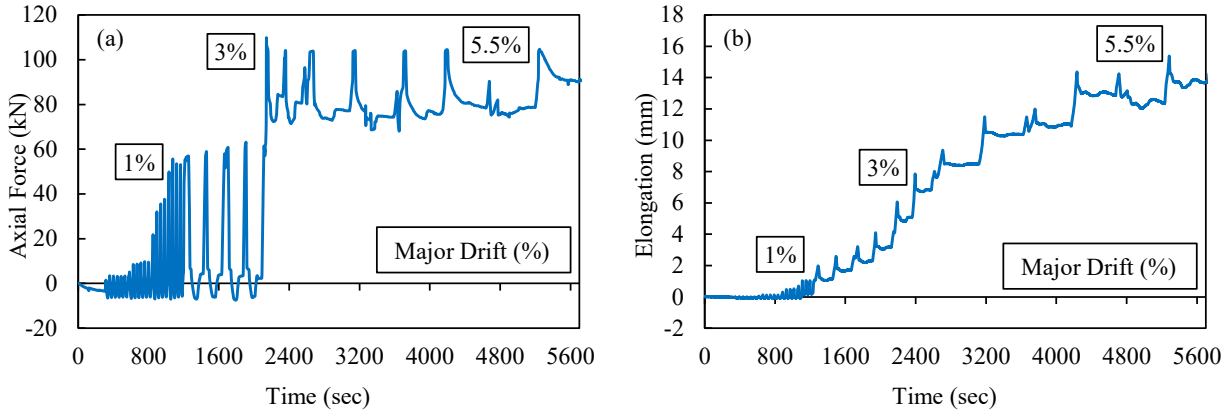

Figure 25 Test 2 Anchor Rod (SE) Results: (a) Anchor Rod Axial Force vs. Time (b) Anchor Rod Elongation vs. Time

(a) *(b)*

Figure 26 Test 2 Results: (a) Test 2 - 3% Drift (Rod Yield) (b) Test 2 - 5.5% Drift (Last Cycle)

4.4 Test 3 – 8-Bolt Configuration (25mm BP)

Figure 27a depicts the base moment generated by the major lateral force in relation to the major base rotation. A maximum base moment of 117.7 kN x m was experienced during the first 2% major drift push cycle in the eastern direction. At the first 1.5% drift cycle a base moment of 114.4 kN x m was computed. In the western direction a maximum moment of -112.8 kN x m occurred during the first 1.5% push drift cycle. It is evident that the test specimen begins to fail at the first 1.5% drift cycle in the western direction and at the first 2% drift cycle in the eastern direction.

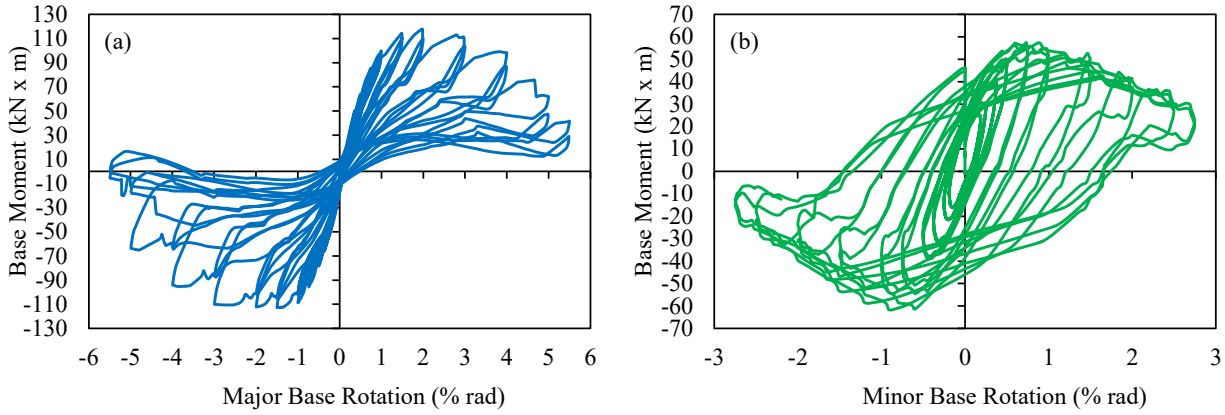

Figure 27 Test 3 Results: (a) Major Base Moment vs. Base Rotation (b) Minor Base Moment vs. Base Rotation

Figure 27b displays the base moment generated by the minor lateral force in relation to the minor base rotation. A maximum base moment of -61.7 kN x m was generated during the first 1.5% minor drift pull cycle in the northern direction. At the first 1% drift cycle a base moment of -61.4 kN x m was also computed. In the southern direction a maximum moment of 57.5 kN x m occurred at the first 0.75% push drift cycle. It is shown that the test specimen begins to lose its ability to resist the forces acting in the minor direction at the first 0.75% minor drift cycle in the southern direction and at the first 1% drift cycle in the northern direction.

Figure 28a depicts a graphical representation of Major Base Moment versus Base Plate Uplift (East). The maximum uplift occurs at the 5.5% lateral drift cycle for both sides of the baseplate. The maximum uplifts are 15.4mm on the west side of the baseplate and 16.4mm on the east. The uplift is less than 4mm for the initial drift cycles up until the end of the 1.5% lateral drift cycle.

At 3% drift the uplift begins to increase more rapidly where the uplift is approximately double the uplift which occurred during the 1.5% drift cycle.

Figure 28b displays Minor Base Moment versus Base Plate Uplift (South). The maximum uplift occurs at the 2.75% minor lateral drift cycle for both sides of the baseplate. The maximum uplifts are 8.5mm for the south side of the baseplate and 8.1mm for the north. The uplift is noted to be less than 2mm for the initial drift cycles up until the end of the 1% lateral drift cycle. After 1% drift the uplift begins to increase more rapidly where the uplift approximately doubles the previous 1% values at the 1.5% major drift cycle.

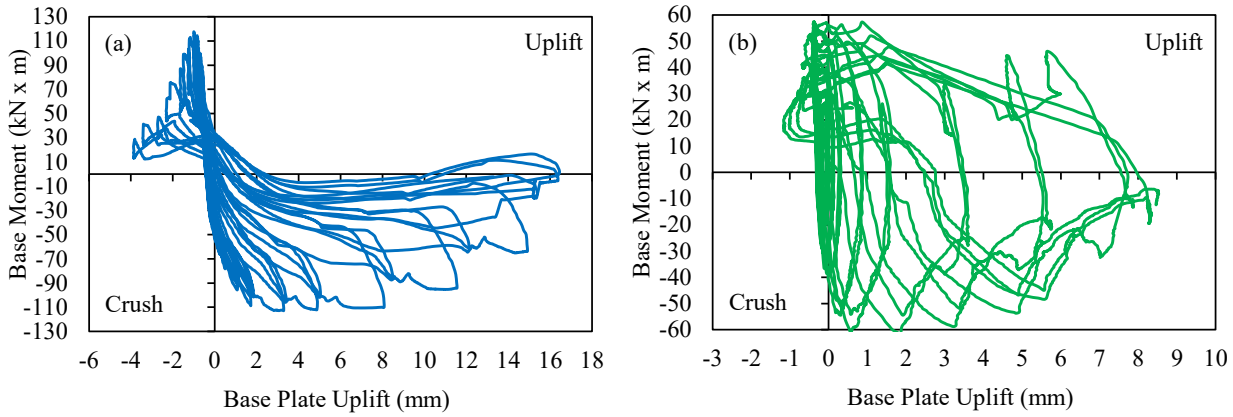

Figure 28 Test 3 Results: (a) Major Base Moment vs. Base Plate Uplift (East) (b) Minor Base Moment vs. Base Plate Uplift (South)

Figures 29a and 29c depicts the axial force for the NW anchor rods recorded throughout the test. It is shown in Figures 29a and 29b that the NW outer rod is engaged elastically at 0.5% major lateral drift, the rod begins to take on more force and begins to stretch at an increased rate after 1% major lateral drift. The NW outer rod yields during the first 1.5% major lateral drift cycle with a peak force of 104.9 kN. At 1.5% drift the outer rod enters its plastic phase. It is shown in Figures 29c and 29d that the NW inner rod is engaged elastically at 0.5% major lateral drift, the rod begins to take greater force and begins to stretch at an increased rate after 1% major lateral drift. The NW inner rod yields during the second 1.5% major lateral drift cycle and achieves a peak force of 106.4 kN at first 2% major drift cycle. At the end of the last 1.5% drift the inner rod enters its plastic phase. Test 3 is categorized as a Weak Connection / Strong Column due to rod yielding. Figures 30a and 30b displays the base connection during the 1.5% and 5% major lateral drift cycles respectively. The NW outer rod is the first rod to yield during the first 1.5%

drift cycle and the first rod to fracture during the 5% drift cycle. The SE and NE outer rods fractured afterwards during the first 5.5% drift cycle.

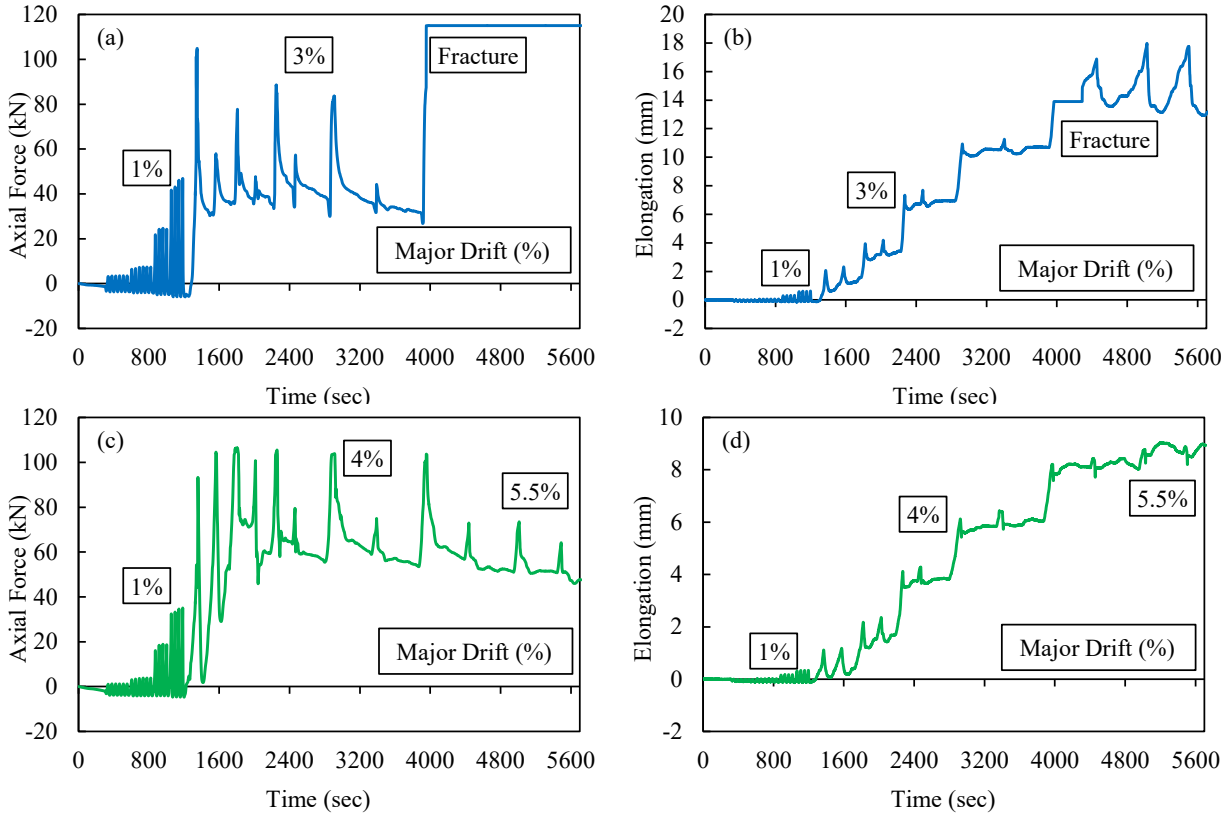

Figure 29 Test 3 Anchor Rod (NW) Results: (a) Outer Anchor Rod Axial Force vs. Time (b) Outer Anchor Rod Elongation vs. Time (c) Inner Anchor Rod Axial Force vs. Time (d) Inner Anchor Rod Elongation vs. Time

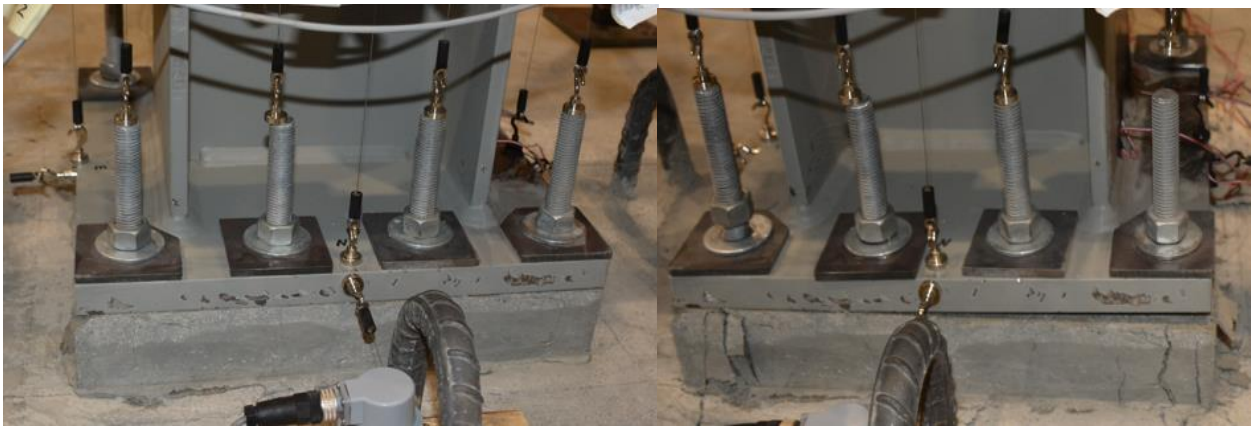

(a) *(b)*

Figure 30 Test 3 Results: (a) Test 3 – 1.5% Drift (NW Outer Rod Yield) (b) Test 3 – 5% Drift (NW Outer Rod Fracture)

4.5 Test 4 – 8-Bolt Configuration (38mm BP)

Figure 31a depicts the base moment generated by the major lateral force in relation to the major base rotation. A maximum base moment of -121 kN x m was experienced during the first 3% drift pull cycle in the western direction. At the first 2% drift cycle a base moment of -120.6 kN x m was computed. In the eastern direction a maximum moment of 117 kN x m occurred during the first 1.5% push drift cycle. It is evident that the test specimen begins to fail at the first 1.5% drift cycle in the eastern direction and at the first 2% drift cycle in the western direction.

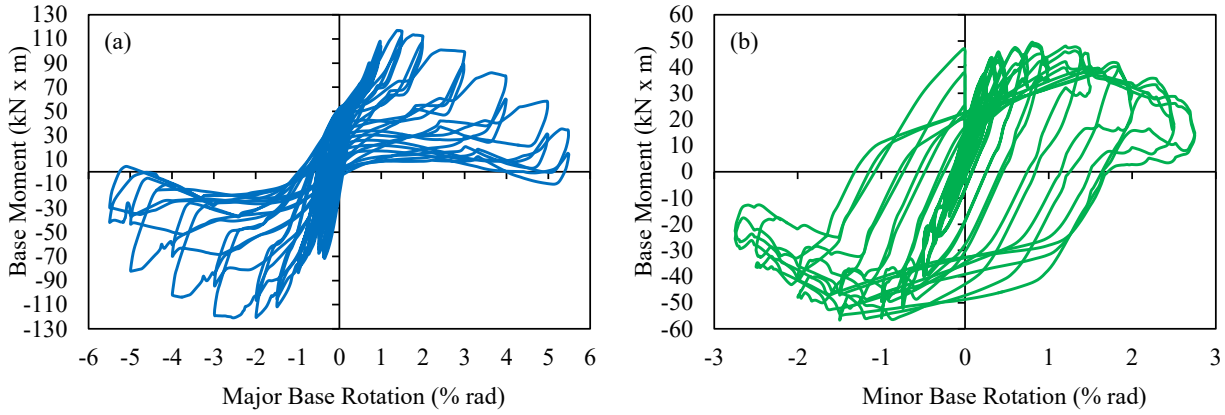

Figure 31 Test 4 Results: (a) Major Base Moment vs. Base Rotation (b) Minor Base Moment vs. Base Rotation

Figure 31b depicts the base moment generated by the minor lateral force in relation to the minor base rotation. A maximum base moment of -56 kN x m was generated during the first 1.5% minor drift pull cycle in the northern direction. At the first 2% drift cycle a base moment of -56 kN x m was also computed. In the southern direction a maximum moment of 50 kN x m occurred at the first 1% push drift cycle. It is shown that the test specimen begins to lose its ability to resist the forces acting in the minor direction at the first 1% minor drift cycle in the southern direction and at the first 1.5% drift cycle in the northern direction.

Figure 32a depicts a graphical representation of Major Base Moment versus Base Plate Uplift (East). The maximum uplift occurs at the 5.5% lateral drift cycle for both sides of the baseplate. The maximum uplifts are 14mm on the west side of the baseplate and 13.4mm on the east. The uplift is less than 3mm for the initial drift cycles up until the end of the 1.5% lateral drift cycle. After 1.5% drift the uplift begins to increase more rapidly similar to the lateral displacement.

Figure 32b displays Minor Base Moment versus Base Plate Uplift (South). The maximum uplift occurs at the 2.75% minor lateral drift cycle for both sides of the baseplate. The maximum uplifts are 6.2mm for both sides of the baseplate. The uplift is noted to be less than 1.5mm for the initial drift cycles up until the end of the 1% lateral drift cycle. After 1% drift the uplift begins to increase more rapidly where the uplift doubles the previous 1% values at the 1.5% drift cycle.

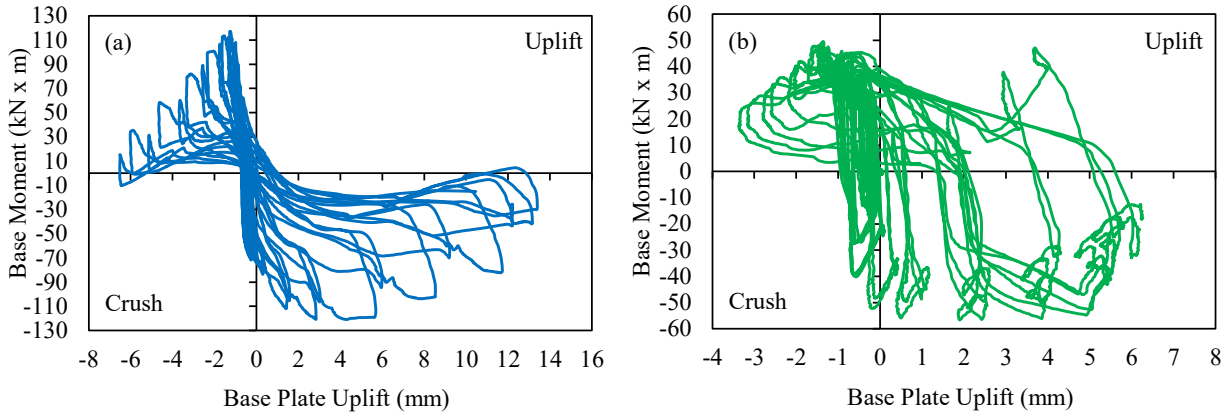

Figure 32 Test 4 Results: (a) Major Base Moment vs. Base Plate Uplift (East) (b) Minor Base Moment vs. Base Plate Uplift (South)

Figures 33a and 33c depicts the axial force for the NW anchor rods recorded throughout the test. It is shown in Figures 33a and 33b that the NW outer rod is engaged elastically at 0.5% major lateral drift, the rod begins to take on more force and begins to stretch at an increased rate after 1% major lateral drift. The NW outer rod yields during the first 1.5% major lateral drift cycle at a peak force of 108.1 kN. At 1.5% drift the outer rod enters its plastic phase. It is shown in Figures 33c and 33d that the NW inner rod is engaged elastically at 0.75% major lateral drift, the rod begins to take greater force and begins to stretch at an increased rate after 1% major lateral drift. The NE outer rod yields during the first 2% major lateral drift cycle at a peak force of 102.6 kN. At 2% drift the inner rod enters its plastic phase. Test 4 is categorized as a Weak Connection / Strong Column due to rod yielding. Figures 34a and 34b displays the base connection during the 2% and 5.5% major lateral drift cycles, respectively.

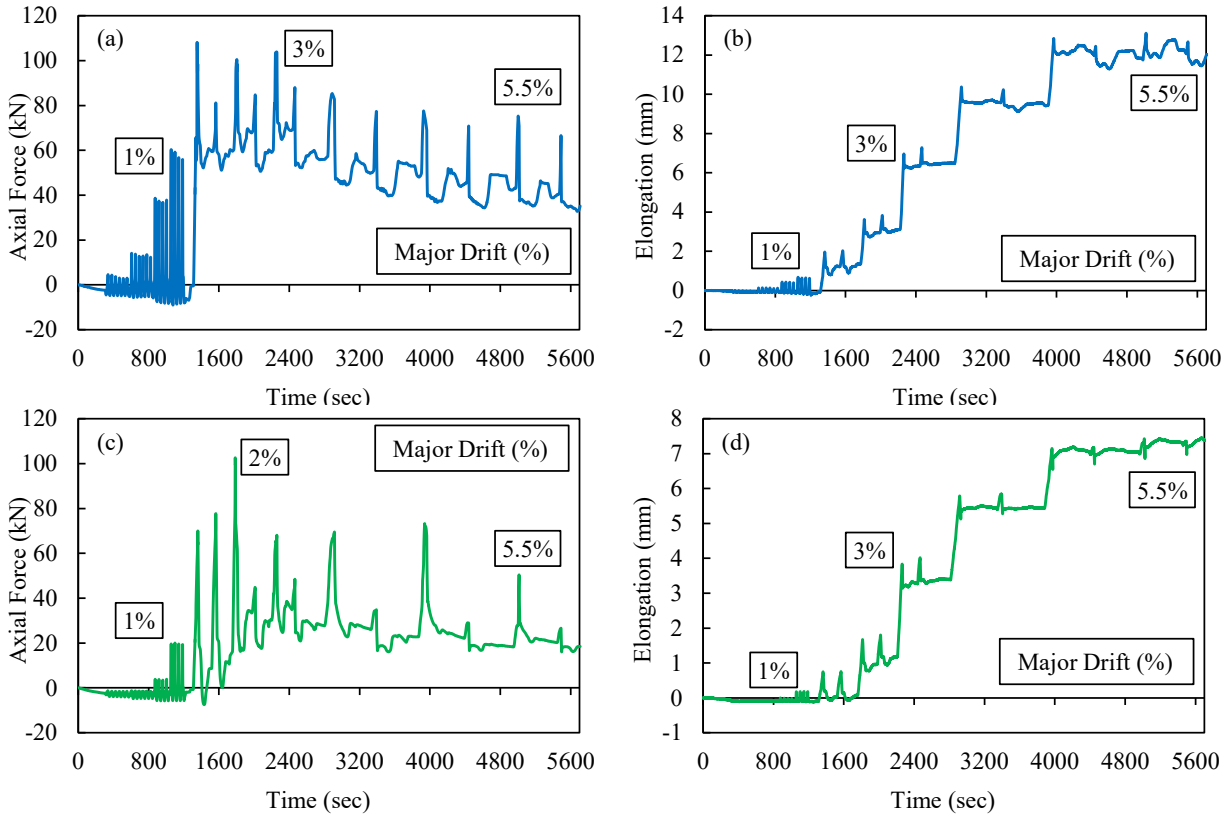

Figure 33 Test 4 Anchor Rod (NW) Results: (a) Outer Anchor Rod Axial Force vs. Time (b) Outer Anchor Rod Elongation vs. Time (c) Inner Anchor Rod Axial Force vs. Time (d) Inner Anchor Rod Elongation vs. Time

(a) *(b)*

Figure 34 Test 4 Results: (a) Test 4 - 2% Drift (NW Inner Rod Yield) (b) Test 4 - 5.5% Drift

Chapter 5 Analysis of Test Results

5.1 General

This chapter uses the results from the experimental testing to conduct an in-depth analysis to help better characterize the behaviour experienced by each of the test specimens. The varying base plate thickness and anchor rod configuration (4-bolt or 8-bolt) will be compared to provide insight into specific CBP connections when subjected to combined axial load and bi-axial bending. This analysis will compare the moment capacity for each of the tests in both the major and minor directions. The analysis will better define the weak connection failure mode for each of the tests by closely comparing the point at which the anchor rods yield in each of the tests. Results will be compared with one another to establish which connection can better resist the base plate uplift condition. The analysis will check and compare the connection strength ratio of each test. Design guide one rectangular stress block method will be checked for each test to see how effectively it can be used for the design of CBP connections subjected to bi-directional lateral loading. The column base rigidity for all the tests will be computed to verify that the weak connections used in the experimental testing are pin connections.

5.2 Moment Capacity

The maximum major base moment for all tests is displayed in Figure 35a in relation to the major lateral drift cycle. The moment capacity of each test helps define which connection configuration is the most ductile and suitable for strong connection design. It is shown that Test 2 experiences greater major base moment up until the end of the 1.5% drift cycles, whereas Test 4 experiences greater base moments afterward. Test 3 maintains a similar moment capacity to Test 2 along the major axis after 1.5% major drift is reached. Figure 35b depicts the maximum minor base moment for all Tests with respect to the minor lateral drift cycle. It is shown that Test 2 experiences greater minor base moments up until 0.5% minor lateral drift cycle, afterwards Test 3 and Test 4 experience greater minor base moments due to the additional rods being located parallel to the major axis.

Test 2 experiences a sudden drop in base moment capacity at the 2% minor drift cycle whereas Test 3 and Test 4 maintain a more stable drop in capacity. Test 4 reaches a maximum major base moment of -121 kN x m during the first 3% drift pull cycle and finishes with a maximum minor

base moment of 52.6 kN x m. Test 2 experiences a major base moment of -116.7 kN x m during the first 2% drift pull cycle and finishes with a maximum minor base moment of 37 kN x m. Test 1 was found to have the least moment capacity in both the major and minor axes of all the tests. It is clear from Figures 35a and 35b that the 8-bolt parallel anchor rod pattern (Tests 3 and 4) has a greater moment capacity than the 4-bolt patterns (Test 1 and Test 2) in both the major and minor directions.

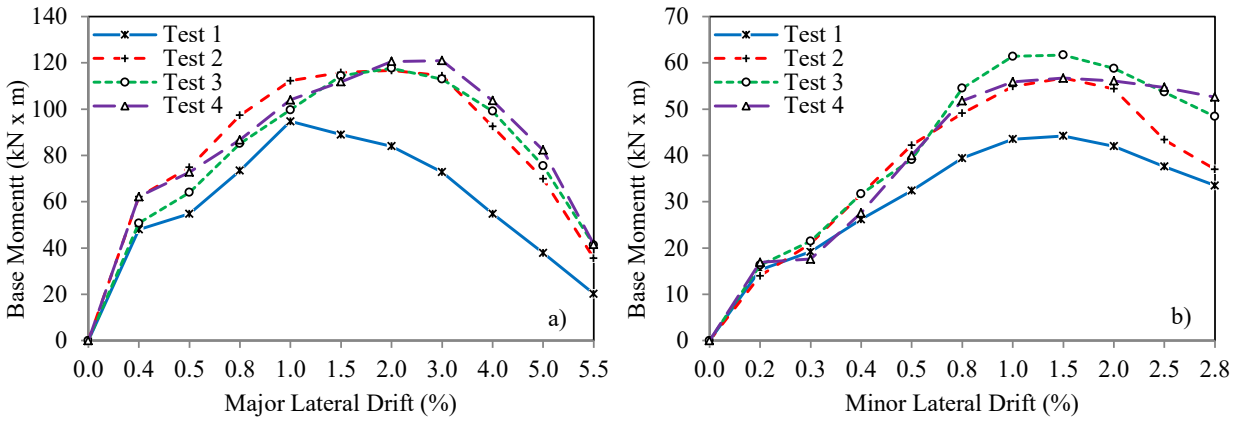

Figure 35 Test Analysis Envelopes: (a) Max Major Base Moment at Specific Major Drift Cycles (Absolute) (b) Max Minor Base Moment at Specific Minor Drift Cycles (Absolute)

Figures 36a - 36d displays the Major Base Moment Backbone envelopes for all experimental tests. The hysteric response shows how Test 4 has the largest curve of all the tests where more energy is dissipated during each of the cycles due to the additional strength provided by the additional rods. It is also evident that Test 2 and Test 4 have very similar responses even though Test 4 has double the amount of rods. This is due to the configuration of the rods, where the additional rods are located parallel to the major loading axis. The points at which base plate uplift and anchor rod yielding occur are labeled in Figures 36a - d for all tests.

Tests 1, 3, and 4 experience base plate uplift engaging during the 1% major drift cycle, where the anchor rods are stretched elastically before yielding at 1.5% major lateral drift. Test 2 experiences anchor yielding at 3% major lateral drift, a couple of cycles later than the rest of the tests, this is mainly due to the increased baseplate thickness (38mm BP) when compared to Test

1(25mm BP). Test 4 outer rods yield at 1.5% major drift whereas the inner rods yield at 2% major drift, whereas both the inner and outer rods in Test 3 yield at 1.5% major drift due to a thinner base plate. Test 3 anchor rod fracture occurred during the beginning of the 5% major lateral drift cycle in the NW direction for Test 3, followed by the fracture of the SE and NE rods near the end of testing during the 5.5% major lateral drift cycles. The fracture of the rods was due to the under-sizing of the baseplate for Test 3, where Test 4 has the same bolt configuration however no fracture was experienced while greater base moments were achieved.

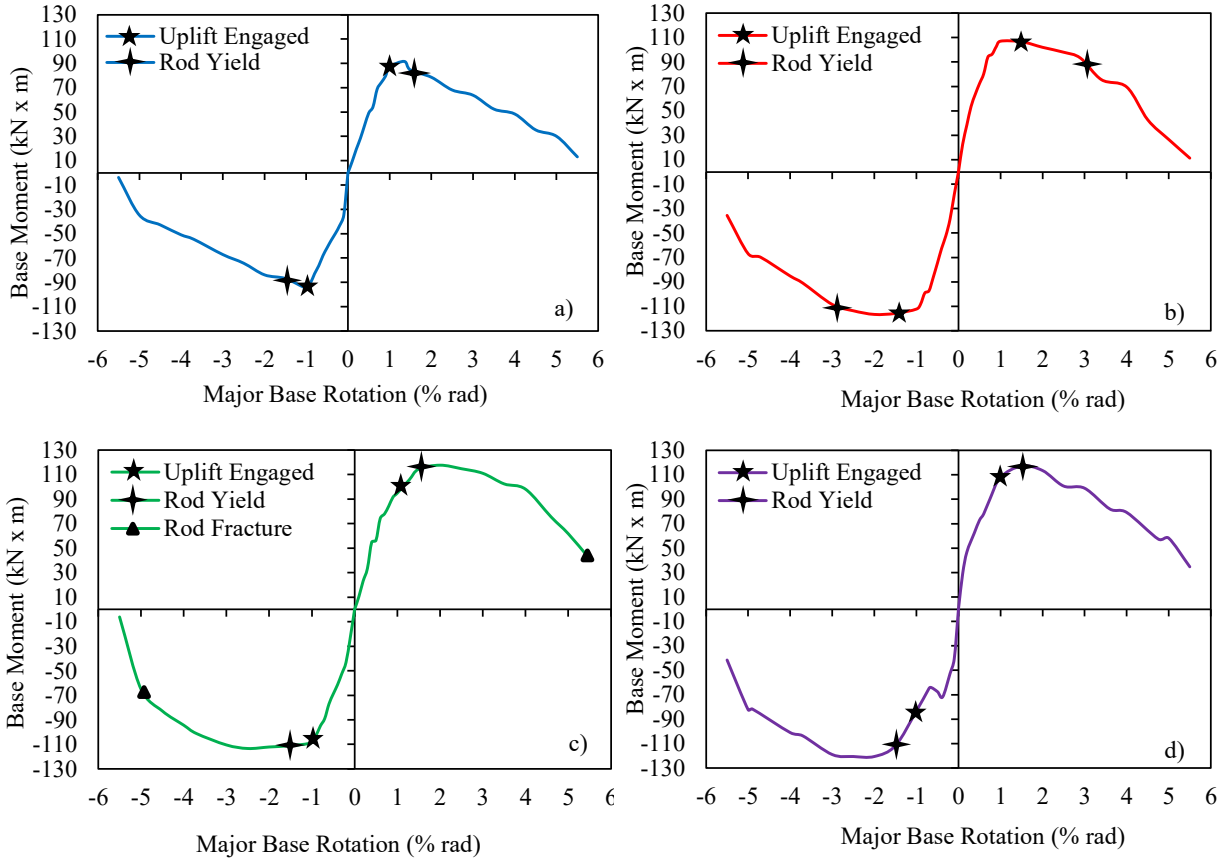

Figure 36 Test Analysis Major Backbone Envelopes: (a) Test 1 Major Base Moment vs. Major Base Rotation (b) Test 2 Major Base Moment vs. Major Base Rotation (c) Test 3 Major Base Moment vs. Major Base Rotation (d) Test 4 Major Base Moment vs. Major Base Rotation

Figures 37a and 37b depict the Minor Base Moment Backbone envelopes for Tests 2 and 4, respectively. The hysteric response shows how Test 4 dissipates more energy in the minor axis during each of the cycles when compared to Test 2, due to the additional rods located parallel to the major axis. It is evident that the two tests have very similar responses even though Test 4 has double the amount of rods. The CBP connections in all the experiments were all engaged along the major axis before minor loading could lead to any cause of failure. Tests 3 and 4 use 8-bolt configurations which have the additional rods located within the depth of the column. This type of configuration strengthens the connection's resistance to minor lateral forces, however, it does not do an adequate job of providing additional resistance to the major loading axis. Therefore once BP uplift is engaged and the anchor rods begin to yield in the major axis the additional rods become redundant for resisting forces in the minor direction and will either yield during the same cycle as the outer rods (BP is undersized) or a cycle after (Test 4) where they are unable to fully contribute to the resistance of the BP uplift in the major axis.

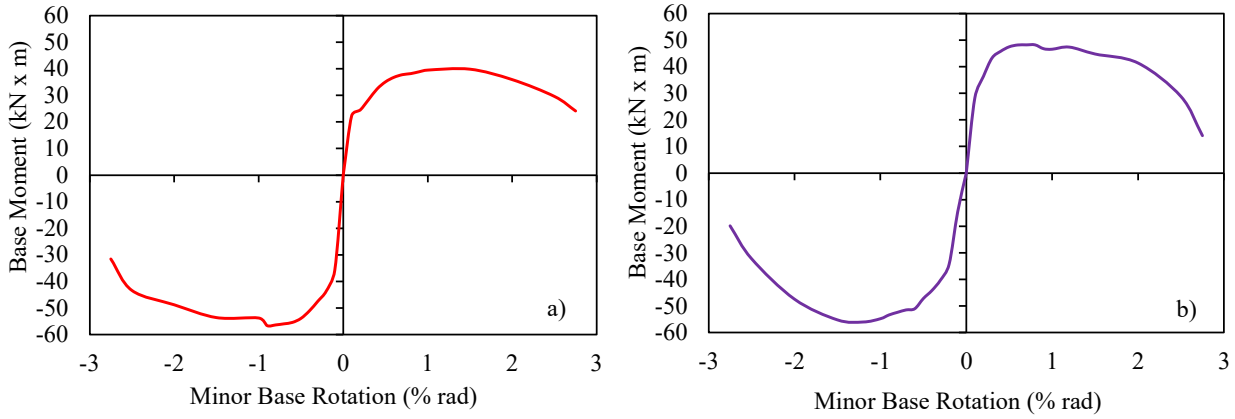

Figure 37 Test Analysis Minor Backbone Envelopes: (a) Test 2 Minor Base Moment vs. Minor Base Rotation (b) Test 4 Minor Base Moment vs. Minor Base Rotation

5.3 Resistance to Base Plate Uplift

The maximum base plate uplift (E-W) envelopes for all tests are displayed in Figure 38a in relation to the major lateral drift cycle. Figure 38b depicts the maximum base plate uplift (N-S) envelopes for all experiments with respect to the minor lateral drift cycle. The resistance to baseplate uplift is shown to help define which connection is most resistant to the uplift condition. The greater a connection can resist base plate uplift the more likely it will be able to achieve its column peak design values. It is shown that Test 2 experiences a maximum major uplift of 16.1mm at the end of the test, whereas Test 4 experiences only 13.9mm uplift. Test 1 experiences increased early major and minor BP uplift up until 2% major drift and 1% minor drift respectively, where the connection is unable to resist uplift as well as the other tests. It is shown that Test 2 experiences a maximum minor uplift of 8.5mm at the end of the test, whereas Test 4 experiences only 6.3mm uplift. It is clear that the 8-bolt pattern has better resistance to base plate uplift than the 4-bolt pattern while still maintaining a greater base moment capacity for both major and minor directions. It is evident that the base plate thickness will have a great influence on the base plate uplift resistance of a connection. Test 3 with a 8-bolt parallel configuration utilizes an under sized baseplate (25mm) and it can be examined that the Test 2 with a 4-bolt configuration with a 38mm baseplate has very similar resistance to base place uplift while maintaining similar moment capacity.

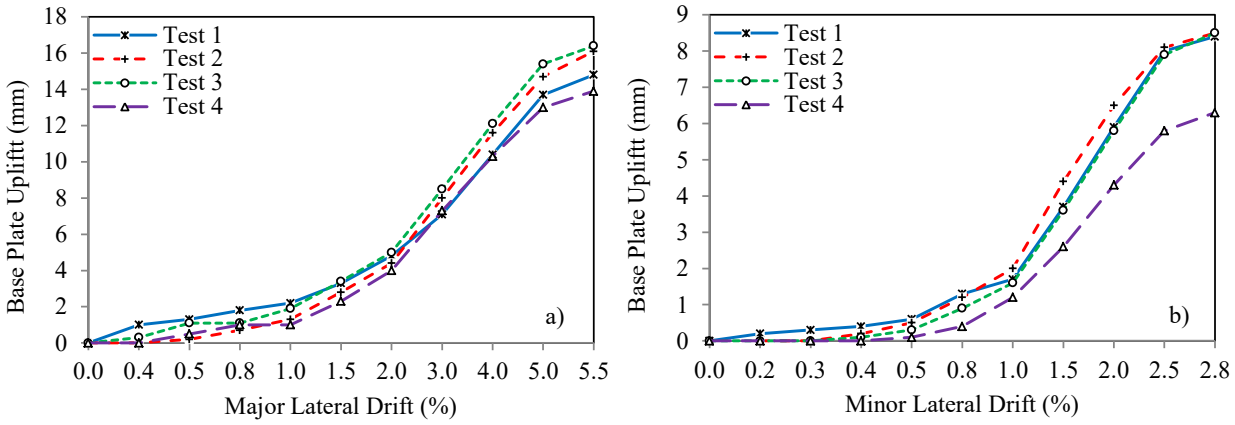

Figure 38 Test Base Plate Uplift Results: (a) BP Uplift Major vs. Major Lateral Drift (b) BP Uplift Minor vs. Major Lateral Drift

5.4 Anchor Rod Yielding – 4-Bolt vs. 8-Bolt (Parallel) Configuration

Tests 2 and 4 will be compared to show the difference in 4-bolt versus 8-bolt (parallel) anchor rod configuration where both tests use a thicker base plate to ensure the main mode of failure is rod yielding. The max anchor rod yield ratio envelopes for Tests 2 and 4 are displayed in Figure 39a in relation to the major lateral drift cycle. It is shown that Test 2 anchor rods are engaged early at 0.5% major lateral drift and begin to yield after 2% drift. Test 2 rods experience greater axial forces than the Test 4 outer rods up until the end of the 1% major drift cycle. It is shown how the outer rods in Test 4 are engaged before the inner rods and yield during the 1.5% major drift cycle, whereas the inner rods yield during the 2% drift cycle. Figure 39b depicts the maximum anchor rod elongation envelopes for Tests 2 and 4 with respect to the major lateral drift cycle. It is shown that Test 2 experiences a max elongation of 15.4mm at the end of the test, whereas Test 4 experiences only 13.7mm of elongation on its outer rods. Test 4 inner rods are more resistant to elongation than the outer rods where the inner rods only experience a max of 7.5mm of elongation. The inner rods in Test 4 provide additional resistance to the base connection allowing the outer rods to take on a greater axial force after the 3% major lateral drift cycle while still being able to better resist elongation when compared to a 4-bolt configuration (Test 2). Both Tests 2 and 4 experience anchor rod yielding as the main mode of failure, which classifies the failure category for both tests as a Weak Connection.

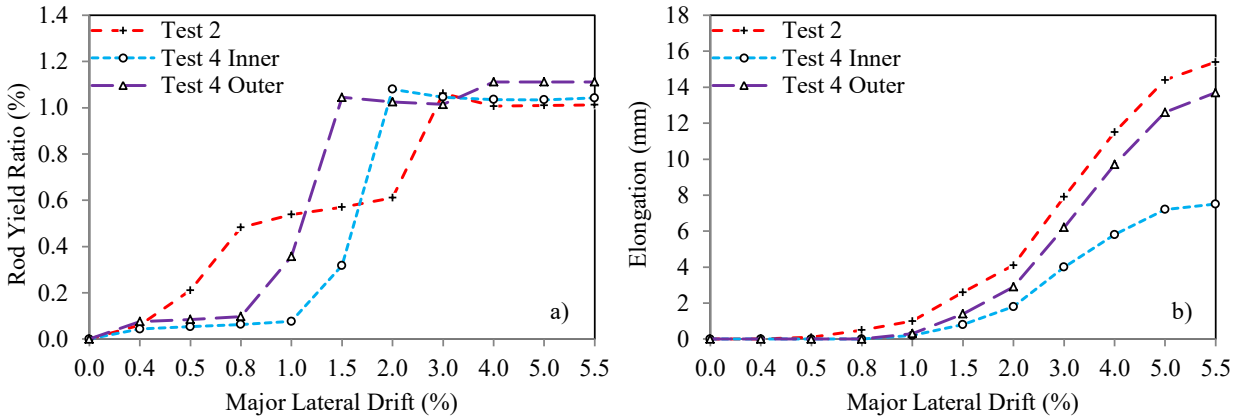

Figure 39 Test 2 and 4 Anchor Rod Envelopes Results: (a) Anchor Rod Axial Force vs. Major Lateral Drift (b) Anchor Rod Elongation vs. Major Lateral Drift

5.5 Connection Strength Ratio Analysis

Table 3 depicts the computed connection strength ratios for each test using Equations 8 and 6. The first column of results uses a ratio of the plastic moment of the column over the plastic moment of the base plate. This check is used to see if the base plate section selected is suitable for the CBP connection design before the anchor rods have been selected. It was found that the 25mm base plates are not suitable for the design using the connection strength ratio, whereas a connection strength ratio of 1.94 was found for both Tests 1 and 3 using column moment over baseplate moment Equation 3. It was found that the 38mm base plates used in Tests 2 and 4 are suitable for design with a ratio of 0.84. The second column of results using T_r represents a conservative design approach taking into consideration the tension resistance of the anchor rods computed from CSA S16-14 which uses a resistance reduction factor of 0.67 (φ_{ar}) for the tension resistance of the rods and reduction factors of 0.9 for the base plate (φ_{bp}) and column (φ_c) plastic moments. This allows for a more conservative design which prioritizes the failure of the anchor rods. The third column of results uses the tension force at which the rods yield to provide a more accurate connection strength ratio comparable to test results. From the results of the second and third columns it is clear that all four tests are classified as weak connections using the connection strength ratio which coincides with the results from the experimental testing. It was found that the connection strength ratio can be used to classify the failure category for all four experimental tests. FEM (Finite Element Model) 7 represents a 4-bolt configuration that utilizes 32mm diameter F1554 anchor rods (Fu = 1010 MPa) which is later presented in a Reliability Analysis within this thesis. As shown in Table 3, FEM 7 is potentially a strong connection.

Table 3 Connection Strength Ratio Analysis

Test #	$\frac{\mathbf{Mp_c}}{\mathbf{Mp_p}(2+\frac{\mathbf{d_c}}{\mathbf{e_b}})}$	$\frac{\mathbf{Mp_c}}{(\mathbf{2Mp_p+T_r d_c})}$	$\frac{\mathbf{Mp_c}}{(\mathbf{2Mp_p+T d_c})}$
Test 1	1.94	4.50	3.67
Test 2	0.84	2.62	2.32
Test 3	1.94	3.39	2.62
Test 4	0.84	2.20	1.85
FEM 7	0.84	1.04	0.83

5.6 Design Guide One - RSB Analysis

Table 4 displays the computed results for Design Guide One RSB approach for calculating the tension force demand for the anchor rods for each CBP configuration used in each experimental test. T_{f1} is calculated using the maximum moment experienced in each experimental test. T_{f2} is calculated using the major column plastic moment which includes a resistance reduction factor φ_c. T_{r1} depicts the calculated anchor rod tension resistances using CSA S16-14 for each of the tests. The tension resistance for a singular 19mm SAE J429 anchor rod (Fu = 428 MPa) is 69 kN. The RSB method does a satisfactory job providing the tension force demand for both the 4-Bolt and 8-Bolt configurations, where all tests fail due to anchor rod yielding. Test 2 has a T_{f1} equal to127.6 kN where the calculated T_{r1} is 138 kN, these values are very close and suggest anchor rod failure may occur. The anchor rod tension force demand calculated using the column plastic moment (T_{f2}) is greater than the rod tension resistances (T_{r1}) for all experimental tests. T_{r2} is the total calculated tension resistance using CSA S16-14 for 32mm F1554 anchor rods (Fu = 1010 MPa) where the resistance of a singular rod is 462.6 kN. The F1554 32mm rods are used later in this study (FEM 7) in a reliability analysis which uses the RSB method to calculate the anchor rod tension force demand for each experiment. It was found that the 8-bolt pattern experiences a sizeable reduction in tension resistance due to the additional rods being placed parallel to the major lateral loading. This causes an additional reduction of 0.72 for resistance of the inner rods which are located within the depth of the column. Even with this reduction applied in design, it was found that the 8-bolt experiments were not able to use the additional strength of the inner rods to efficiently resist the base plate uplift condition in the major axis where the outer rods are engaged before the inner rods can help resist the tension demand.

Table 4 Design Guide One RSB Analysis

Test #	T_{f1} (kN)	T_{r1} (kN)	T_{f2} (kN)	T_{r2} (kN)
Test 1	94.6	138	863.4	925.2
Test 2	127.6	138	863.4	925.2
Test 3	132.9	237.5	863.4	1590.7
Test 4	146.5	237.5	863.4	1590.7

5.7 Column Base Connection Rigidity Analysis

According to the rotational stiffness (K_θ) values shown in Table 5, Tests 2, 3 and 4 connections can be classified as fully pinned along the major axis since the base rotational stiffness is less than 0.5(EI/H) which is 8828 kN x m / rad. Test 1 major base connection stiffness is very close to the 0.5(EI/H) limit where the peak base moment is the least out of all tests and is achieved at the lowest base rotation, this should result in a very poor rigidity check, where the result should not be classified as a semi-rigid connection. Test 1 is the worst connection out of all the experimental testing yet is the only test that classifies as a semi-rigid connection in the major direction. The rigidity checks in the minor direction for all tests are found to be classified as semi-rigid connections where the base rotational stiffness is less than 0.5(EI/H) which is 2640 kN x m / rad. Test 1minor base connection stiffness is bordering on the 0.5(EI/H) lower limit where it is questionable whether or not the connection should be classified as a semi-rigid connection along the minor axis. Test 4 was the strongest connection out of all the experimental testing and was the most rigid of all connections having the most anchor rods and thickest base plate which means it should technically have the best base rotational stiffness. However this is not the case, Test 4 has the lowest calculated major base connection stiffness of all the tests and also has a lower minor base rotational stiffness than Test 2 which is only a 4-Bolt Test. Therefore more work needs to be done to adjust the column base connection rigidity check to account for additional anchor rods and the thickness of the base plate (similar to connection strength ratio).

Table 5 Column Base Rigidity Analysis

Test #	θ (% rad)	M_{Max} (kN x m)	K_θ (kN x m / rad)	Rigidity
Test 1 Major	1	94.7	9470	Semi - Rigid
Test 1 Minor	1.5	44.3	2946	Semi - Rigid
Test 2 Major	2	116.7	5835	Pin
Test 2 Minor	0.9	56.7	6300	Semi-Rigid
Test 3 Major	2	117.7	5885	Pin
Test 3 Minor	0.9	61.7	6855	Semi-Rigid
Test 4 Major	2.5	121	4840	Pin
Test 4 Minor	1.5	56.7	3780	Semi-Rigid

Chapter 6 Finite Element Modeling and Reliability Analysis

6.1 FEM Validation

6.1.1 Background

In this research, Test 2 experimental results were used to create a FEM validation using ABAQUS software. Test 2 was used for FEM validation since this specimen showed expected behaviour and all component responses were captured accurately. Moreover, Test 2 had four anchor rods with a 38mm base plate which is a common configuration for CBP connections in steel buildings. The validation model uses the same bi-directional lateral loading protocol as the experiments where some modification had been made to shorten the amount of cycles in the beginning of the test so the software could accurately predict the experimental results. The model accurately captures the lateral forces applied to the column, base plate uplift, anchor rod elongation, and anchor rod axial forces. Test 2 failure is caused by yielding of the anchor rods which classifies it as a weak connection. The parameters captured in the FEM validation show very similar results to the experimental test and can be used to help predict and justify the type of failure for specific CBP connection configurations. The Test 2 FEM validation model will be used as the base model for a 4-Bolt CBP configuration parametric study where anchor rod properties will be adjusted until a strong connection failure is reached. The results from the FEM parametric study will be used to conduct a reliability analysis on 4-Bolt CBP configurations.

6.1.2 ABAQUS Model Properties

The FEM validation model uses the same material properties for all components as displayed in Table 2. The fillet welds were modeled with a yield strength (F_y) of 524 MPa and ultimate strength (F_u) of 572 MPa. The nuts and washers were modeled as a linear elastic perfectly plastic component with a yield strength of 345 MPa. All components were created as 3D Deformable Solid Parts using Linear Hexahedral (C38DR) mesh elements. Cyclic hardening parameters were obtained for the base plate and column through trials to achieve similar behaviour to experimental testing. The program was set to run as a dynamic implicit analysis step type with quasi-static application and use half cyclic data method where the plastic strain parameters were incorporated for the isotropic properties. For the kinematic properties for the base plate and column, an equivalent stress was set to the yield strength of the material with Q-infinity values of 172 and 90 and Hardening parameter ~~–b~~" values of 2 and 12 respectively based on trials. The

base plate and grout were modeled using 12.5mm cubic mesh, the column uses 10mm cubic mesh, the rods use 5mm mesh, the nuts and washers use 3mm cubic mesh, and the fillet welds use 12mm mesh. A general surface interaction was created for the entire model where a friction coefficient of 0.45 was utilized to act as the grout to steel interaction. A specific surface interaction was applied between the base plate and washers where a friction coefficient of 0.8 was used to define the steel-to-steel contact. Tie contact restraints were utilized for connecting the welds to the BP and column and the nuts to the anchor rods. A fixed boundary condition was applied to base of the grout and the bottom ends of the anchor rods located at the base of the grout in the models. A multiple point constraint was applied to the top of the column to allow for the major and minor lateral displacements to be applied simultaneously.

6.1.3 Bi-Directional Lateral Loading Protocol

The bi-directional lateral loading protocol used in the Test 2 experiment was modified to run implicitly by reducing the amount of repeat early drift cycles up until 1% major drift and by transforming the explicit test time to implicit step-based time (unitless or incremental). This was achieved by only using one cycle per drift up until the end of the 1% major drift cycle as show in Figure 40a, this allowed the program to run much efficiently and produce more accurate results. Figure 40a displays the major displacement vs. step time which was used for the model. Figure 40b depicts the minor displacement vs. step time for the model. Inputting the lateral displacements into ABAQUS correctly using this method was crucial for obtaining accurate results. The displacements are inputted into ABAQUS deterministically before the job is run.

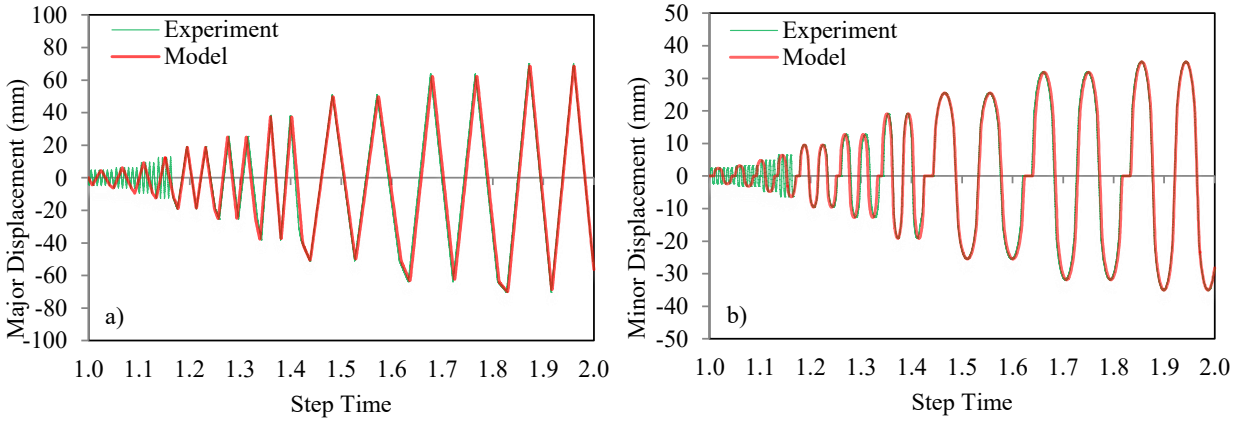

Figure 40 FEM Bi-Directional Lateral Loading Protocol (a) Major Displacement vs. Step Time (b) Minor Displacement vs. Step Time

6.1.4 Major and Minor Lateral Forces

The FEM validation model was programmed to capture the lateral forces applied to the top of the column in both the major and minor directions. Figure 41a and 41b depicts the results from the model in comparison to the experiment for both the major and minor lateral forces. It is clear from the figures that the FEM model does a satisfactory job at predicting the forces occurring during each drift cycle. In order to capture these results accurately a set of integrated surface output sections were utilized to record the lateral forces occurring in the area where the lateral actuator would be applying the loads in the experiment.

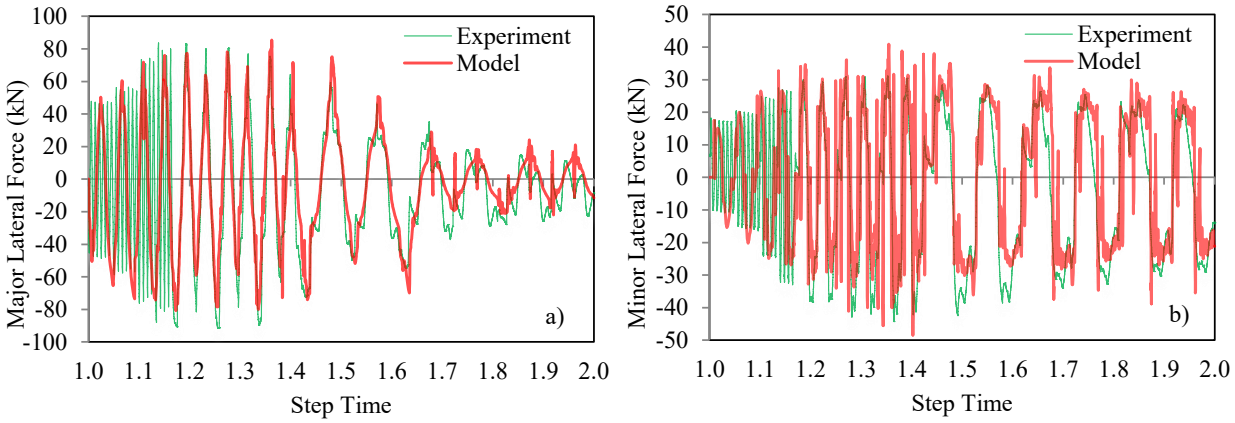

Figure 41 FEM Lateral Forces (a) Major Lateral Force vs. Step Time (b) Minor Lateral Force vs. Step Time

6.1.5 Base Plate Uplift

The FEM validation model was able to accurately capture the maximum base plate uplift on all sides of the base plate. In addition to capturing the uplift, the crushing of the grout at the edges is also captured. The grout was programmed to act as a spring. Once the base plate uplift condition is engaged, a trigger is set based on the material strength properties of the grout/concrete to allow displacement (crushing) to occur when running an implicit analysis. As shown in Figures 42a and 42b, the base plate uplift and grout crushing occurring along the major axis (East-West) are captured and the results are almost exact. The results show how the model is unable to capture the early signs of the grout crushing when the base plate uplift is less than 4mm. After 4mm of base plate uplift the crushing in the model is triggered and accurate results are captured for the remainder of the test.

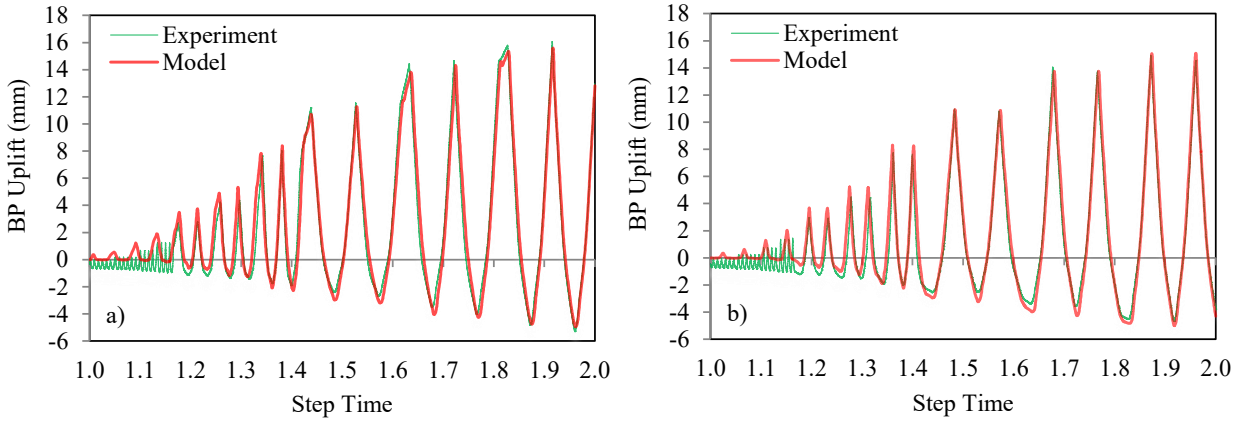

Figure 42 FEM Base Plate Uplift (a) BP Uplift (East) vs. Step Time (b) BP Uplift (West) vs. Step Time

As depicted in Figures 43a and 43b, the base plate uplift and grout crushing occurring along the minor axis (North-South) is captured and the results are quite satisfactory. It is shown how the model is unable to capture the early signs of the grout crushing when the base plate uplift is less than 4mm. After 4mm of base plate uplift the crushing in the model is triggered and accurate results are captured for the remainder of the test.

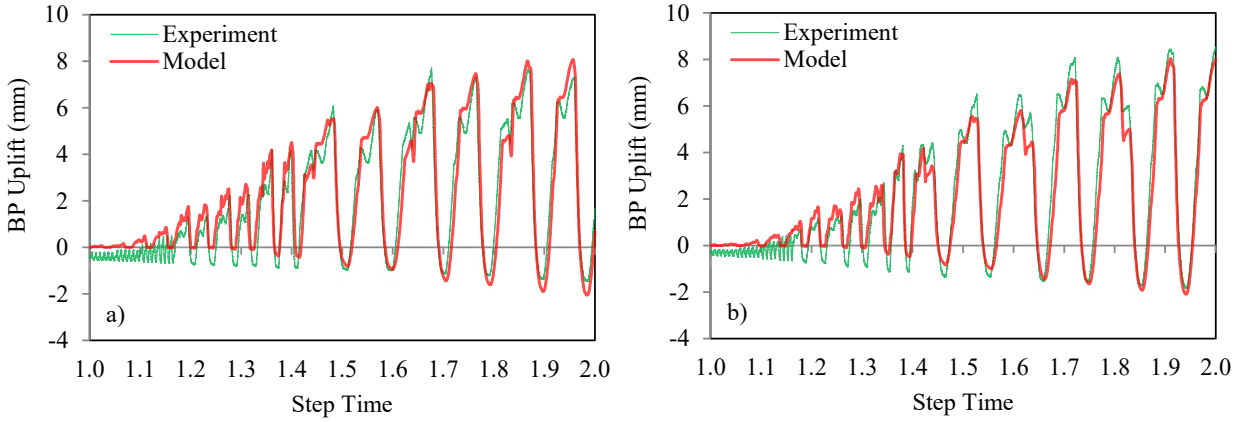

Figure 43 FEM Base Plate Uplift (a) BP Uplift (North) vs. Step Time (b) BP Uplift (South) vs. Step Time

6.1.6 Anchor Rod Elongation

The validation model was developed to obtain the maximum anchor rod elongations for all four rods. It was found that the results are satisfactory where the model captures the results within 1.5mm of the experiment during the entirety of the test. The elongation peaks are all very close for each drift cycle where the model can predict the later drift cycle elongations more accurately. The anchor rod elongation for the North-West and South-East rods are displayed in Figures 44a and 44b respectively.

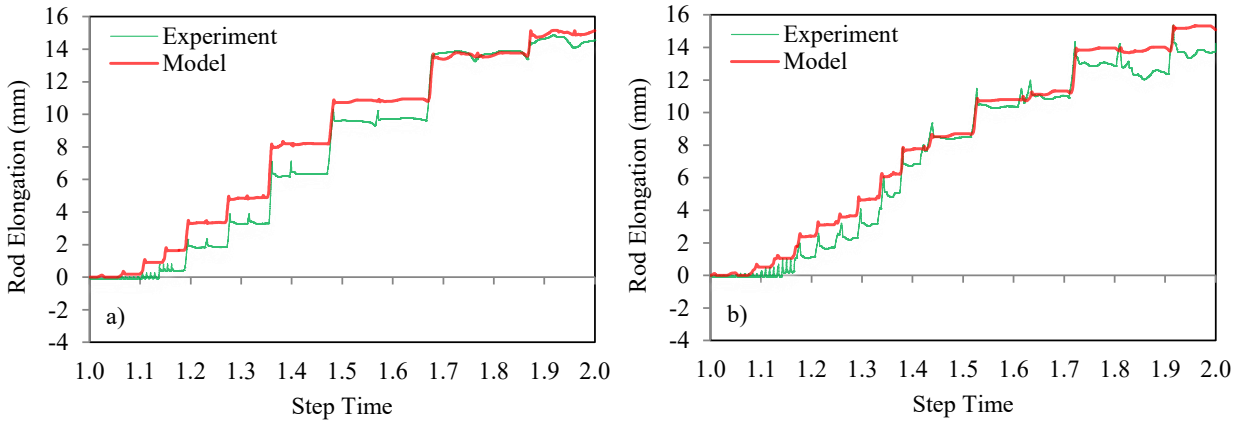

Figure 44 FEM Anchor Rod Elongation (a) NW Rod Elongation vs. Step time (b) SE Rod Elongation vs. Step time

6.1.7 Anchor Rod Axial Force

The FEM validation was programmed to capture anchor rod axial force for all the rods. Integrated surface section outputs were utilized in ABAQUS to capture the results accurately. It was found that the model can accurately predict the forces in the rods for the entirety of the test. The model is picking up axial force in the rods during the early stages (before 1% major lateral drift) of the test whereas in the experiment the strain gauges are embedded below the concrete and are not engaging as soon as the model. Once the rods are engaged in the experiment the model captures the axial forces more accurately during the elastic phase between 1 and 3% major lateral drift (before 1.5 step time). The model then captures when the rod yields and enters its plastic phase. In the model, the axial force drops back to zero in the plastic phase, whereas strain gauges were used to capture the vertical strain of the rod and then converted to axial forces for

the experiment. Figure 45a depicts the axial force recorded in the South-West anchor rod. Figure 45b displays the corresponding anchor rod elongation for the South-West rod. Figure 46 displays a comparison of the experiment to the finite element validation model at the end of testing.

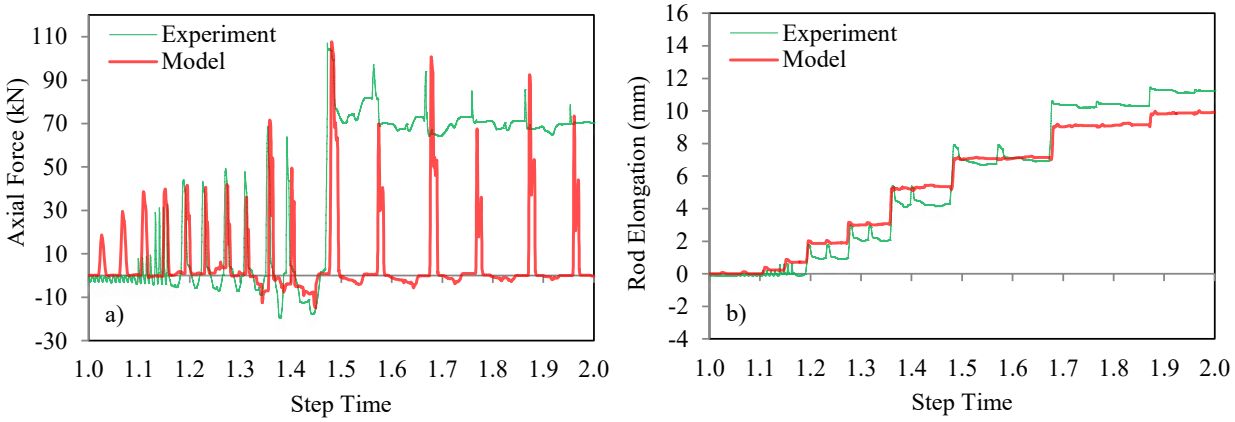

Figure 45 FEM South West Anchor Rod (a) SW Anchor Rod Axial Force vs. Step Time (b) SW Anchor Rod Elongation vs. Step Time

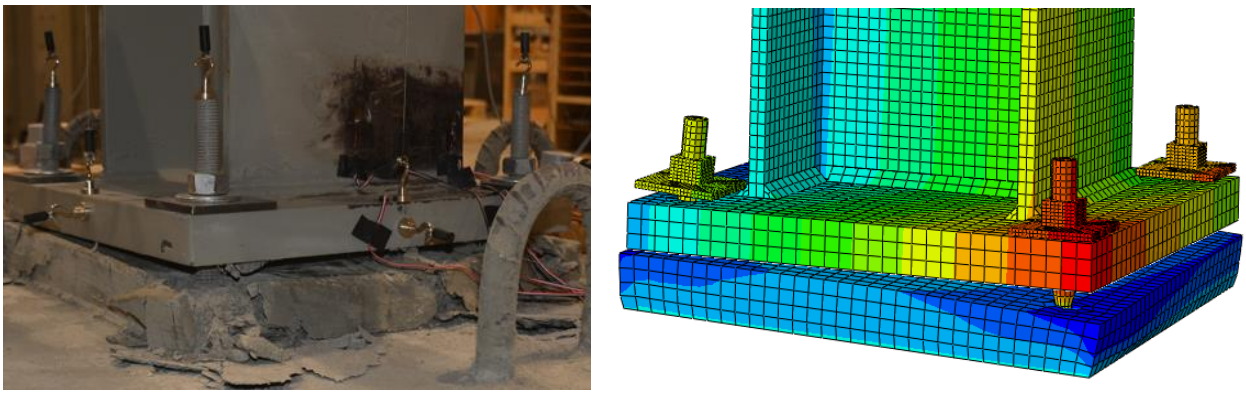

Figure 46 FEM Test 2 Validation – Experiment vs. FEM (End of Test)

6.2 Reliability Analysis

6.2.1 General

This section presents an extensive 4-Bolt CBP connection Reliability Analysis using Monte Carlo simulation in combination with experimental and FEM results. The resistance and demand equations are presented from which the four performance equations relating to CBP connection failure are derived. A table of the random variables and associated probabilistic values pertaining to specific CBP connection components is showcased where the values are used directly in a series of Monte Carlo Simulations using MATLAB. Results have been displayed in a table to compare the failure modes and evaluate the accuracy of the MCS Reliability Analysis. The results from this analysis can be used to help provide design guidance for CBP connections subjected to combined axial and bi-directional lateral loading.

Monte Carlo Simulation requires defining a set of random variables (i.e., Mean, Standard Deviation, Distribution), then generates a set of random variables (random number between 0 and 1) based on the number of iterations required. The collection of random variables generated can be used in performance equations (i.e., Z = Resistance - Demand) to predict the probability of failure. For resistance against demand, you set the program to record the number of times the resistance is less than the demand for each failure mode (performance equation), then divide that value by the number of iterations to obtain the probability of failure. The probability of failure can be converted into a reliability index through Cumulative Distribution Function inversing. For the Monte Carlo Simulation used in this study, examples from J. Deng's Structural Reliability Lecture notes (2023) were closely followed to develop a MATLAB program to run one million iterations for each test efficiently. The program was written to use four performance equations to define the failure mode/modes of the specific tests. The probability of failures was calculated for each failure mode (performance equation), then converted to reliability coefficients and checked against the experiments and models to see if the results (failure categories) align.

6.2.2 Resistance and Demand Equations

Resistance Equations 1-4 and RSB Equations 10-16 will be used in a CBP Connection Monte Carlo Simulation Reliability Analysis as the resistance and demand the components must meet to prevent failure. The Moment (M) and Axial Force (P) used in Equations (10-12) will be inputted into the program as deterministic values, which are obtained from experimental and FEM results.

The elastic section modulus (Z_x or Z_y) used to calculate the plastic moment resistance of the column and base plate incorporates the specific material geometry into its calculation, allowing for the use of random variables to account for its uncertainty. The yield/ultimate strength of the components used in a base connection are all subject to uncertainty, allowing us to conduct a probabilistic reliability analysis using random variables to capture the uncertainty.

6.2.3 Random Variables

A total of 12 random variables were used for all Monte Carlo Simulations. These variables are based on the geometric and material properties of the steel column, base plate, anchor rods, and concrete. Table 6 below depicts the random variables used for all simulations. The COVs and distributions were taken directly from Song (2021), where similar materials were used. The tests are varied by base plate thickness, anchor rod diameter, and anchor rod grade to capture the various failure modes of exposed column base connections. The means for the geometric properties use mm as units, whereas the material strength properties are in MPa units.

Table 6 Random Variables

RV	Random Variable	Annotation	Mean(s)	COV	Distribution
1	Depth of Column	**Dc**	253	0.002	Normal
2	Column Flange Width	**Bf**	264	0.004	Normal
3	Column Flange Thickness	**Tf**	14.2	0.025	Normal
4	Column Web Thickness	**Tw**	8.6	0.025	Normal
5	Base Plate Length/Width	**Bp**	406.4	0.025	Normal
6	Base Plate Edge Distance	**Bg**	38	0.05	Normal
7	Base Plate Thickness	**BTf**	25, 38	0.03	Normal
8	Anchor Rod Diameter	**Dr**	19, 25, 32	0.085	Normal
9	Column Yield Strength	**CFy**	390	0.05	Normal
10	Base Plate Yield Strength	**BFy**	366	0.07	Normal
11	Concrete Compressive Strength	**fc**	32.7	0.145	Normal
12	Anchor Rod Ultimate Strength	**RFu**	428, 1010	0.16	Log-Normal

6.2.4 Performance Equations

The Monte Carlo Simulations were programmed to capture four failure modes related to CBP connections. The first failure mode (g1) shown in Equation 23 is due to an expected plastic hinge forming in the column flange due to the moment in the test exceeding the plastic moment

capacity of the column in the major direction. The second failure mode (g2) shown in Equation 24 is caused by a plastic moment forming in the column web. Both the first and second failure modes are associated with a Strong Connection / Weak Column failure category where the column can reach its peak design values. The max moments used for g1 and g2 are obtained from experimental/FEM test results deterministically. Failure modes g1 and g2 are the most desirable for column base connection design. Failure mode g3, shown in Equation 25, is related directly to anchor rod yielding; this type of failure contributes to a Strong Column / Weak connection failure. Failure mode g4, shown in Equation 26, is caused by base plate yielding, which is classified as a Strong Column / Weak Connection failure mode. All the performance equations experience failure when g( ) is less than zero. The program records the number of times the equation computes less than zero answers and then divides by the number of iterations to generate the probability of failure for each mode.

$$\boldsymbol{g1 = M_{px,colm} - M_x Max} \tag{23}$$

$$\boldsymbol{g2 = M_{py,colm} - M_y Max} \tag{24}$$

$$\boldsymbol{g3 = T_r - T_f} \tag{25}$$

$$\boldsymbol{g4 = M_{p,plate} - M_{f,plate}} \tag{26}$$

6.2.5 MCS Test Matrix

Table 7 Test Matrix for Monte Carlo Simulations

Test #	**BP (mm)**	**Bolt Pattern**	**Axial Load (kN)**	**M_{MAX} (kN x m)**	**M_{Xmax} (kN x m)**	**M_{Ymax} (kN x m)**	**Rod F_u (MPa)**	**Rod Dia.(mm)**
1	407x407x**25**	4	400	108	94.7	44.3	428	19
2	407x407x**38**	4	400	119	117	57	428	19
3	407x407x**25**	4	400	177.3	163.4	77.1	1010	19
4	407x407x**38**	4	400	170.5	166.3	72.2	1010	19
5	407x407x**25**	4	400	196.1	183.1	91	1010	25
6	407x407x**38**	4	400	240	230	100	1010	25
7	407x407x**38**	4	400	281	233.3	122.6	1010	32

The test matrix in Table 7 displays the differences between all the tests run in the Monte Carlo Simulations. Tests 1 and 2 results are from our experimentation and Tests 3 - 5 results are from the FEM 4-Bolt CBP connection parametric study conducted based on the Test 2 FEM validation. All tests use 4-Bolt anchor rod patterns with a constant axial load of 400 kN. The base plate thickness varied throughout the tests (25 or 38mm), rod diameter increased (19 - 32mm), and rod grade increased (428 - 1010 MPa) to capture the effects of the main components involved in the column base connection failure. The M_{MAX} is the combined moment experienced throughout all the tests and is used to input the (M) in Equation 12 to calculate the tension demand. The M_{Xmax} and M_{Ymax} values are the maximum moments experienced in each corresponding direction. The maximum moments are obtained from experimental and FEM test results.

6.2.6 Results and Conclusions

Table 8 Test Results for Monte Carlo Simulations

Test #	pF_1 (%)	β_1	pF_2 (%)	β_2	pF_3 (%)	β_3	pF_4 (%)	β_4	Failure Mode (MCS)	Failure Mode (Experiment)
1	0	-	0	-	17.7	0.93	0	-	Rods Yield	Rods Yield
2	0	-	0	-	58.8	-0.2	0	-	Rods Yield	Rods Yield
3	0	-	0	-	61.5	-0.3	46.9	0.08	Rods & BP	Rods & BP
4	0	-	0	-	49.7	7e-3	0	-	Rods Yield	Rods Yield
5	2e-3	4.12	3e-3	4.01	11	1.23	93.8	-1.54	Rods & BP	Rods & BP
6	35.4	0.38	0.46	2.60	54	-0.1	0.13	3.02	Balanced	Balanced
7	45.4	0.12	81.3	-0.89	17.2	0.95	17.3	0.94	Colm Yield	Colm Yield

Table 8 depicts the results from the series of Monte Carlo Simulations. (pF_1) relates to the probability of failure for the column in the major axis (flange buckling), where (pF_2) is the probability of failure for the column web buckling (minor axis). (pF_3) is the probability of failure directly related to anchor rod yielding, and (pF_4) is the probability of failure due to base plate yielding. The corresponding reliability indices (β) are given for each failure mode. Modification was needed to achieve a reasonable reliability analysis that aligns with the experimental results. It was found that the resistance equations required a reduction factor to obtain a satisfactory probability of failure results for the four failure modes. Equation 3 uses a reduction factor (φ_{ar})

equal to 0.67. It was found that the column and base plate resistance equations would also need an increased reduction factor to use the design guide one approach for reliability analysis of the experiments. Through trials, it was found that a reduction factor of 0.60 works well when applied to all the steel components (anchor rods, base plate, and column) utilized in the column base connection design.

Table 8 shows how the modified Monte Carlo Simulations can predict the failure modes with some accuracy. For Tests 1 and 2, it is clear that the yielding of the anchor rods was the cause of the failure, which categorizes the failure as a Weak Connection. Test 2 results show a negative reliability index for the anchor rod failure mode, and this reveals that the rods will be the primary failure mode since it is more likely for the rods to fail than not. In Test 3, it is shown how the base plate and anchor rods yield, which classifies the failure as a Weak Connection. With another negative reliability index for the anchor rods and a very low index for the BP, it is safe to say that rods and base plates should yield simultaneously. Test 4 is a weak connection failure (49.7%- pF3) where the rods yield before the other components.

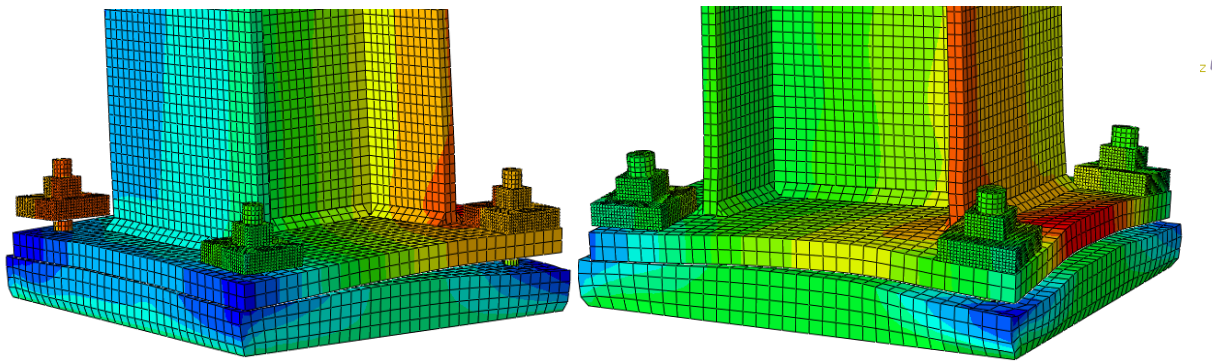

(a) *(b)*

Figure 47 Test Failures-Weak Connection-Rod and BP Yielding: (a) Test 3 (b) Test 5

Figure 47 shows the FEM results for Tests 3 and 5. It is clear from the figure that both tests experience anchor rod yielding as the primary failure mode combined with base plate yielding. There is no sign of buckling in the flange or web of the column in Figure 47a and minimal bending in the flange in 47b, which classifies both connections as a Weak Connection / Strong Column. Test 5 would be the strongest of the weak connections where the reliability indices for the column major and minor buckling modes are above 4.00. It is interesting to note how the

baseplate failure mode is the governing mode to define Test 5 as a weak connection, whereas in Test 6, the baseplate is increased to 38mm, and the failure mode becomes a balanced failure due to the simultaneous yielding of the column flange and anchor rods. It is clear from the results that the 38mm base plate plays a crucial role in allowing the baseplate to reach a more desirable failure mode. When the 25mm base plate is used, the column cannot reach its peak design values, and the rods will yield before the column. This is not ideal, for the rods are large enough to achieve a balanced failure; however, the yielding of the base plate reduces the rods' capacity where the column cannot engage plastically.

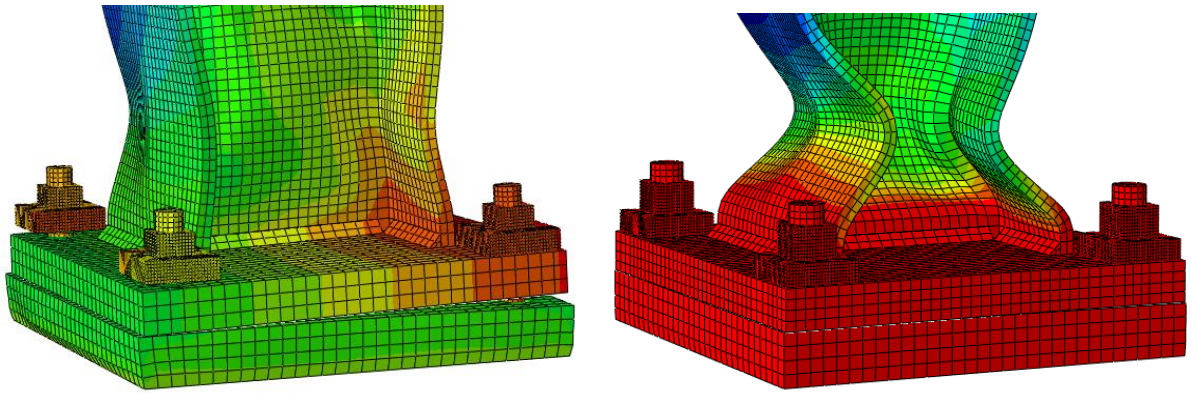

(a) *(b)*

Figure 48 Test Failures: Balanced and Strong Connection: (a) Test 6 (b) Test 7

Figure 48 displays FEM results for Tests 6 and 7. It is shown how Test 6 experiences buckling in its flanges as well as yielding in the anchor rods. This coincides with the Test 6 Monte Carlo simulation results, where a probability of failure of 35.4% was calculated for the column flange buckling and a probability of failure of 54% for the anchor rod yielding. It is also noted that a reliability index of 3 was found for the base plate yield failure mode, which tells us that the base plate thickness is a good choice.

Figure 48b depicts the FEM results for Test 7. This model exhibits a Strong Connection / Weak Column, where buckling in the flanges and web occurs before the baseplate and anchor rods yield. FEM Test 7 uses the thickest rods (32mm) with the strongest grade (F_u =1010 MPa) compared to the other tests. Other tests which use the 38mm base plate incorporate rods of smaller diameter, which does not allow the connection to sustain long enough for the plastic

hinge to initiate in the column flanges/web. The Monte Carlo Simulation does a satisfactory job at categorizing the failure for Test 7, where a probability of failure of 45.4% and 81.3% was computed for the column's major and minor axis buckling, respectively.

The series of Monte Carlo Simulations does a satisfactory job of conducting a reliability analysis on various exposed column base connections subjected to combined axial and bi-directional lateral loading. Further research is required to analyze the design guideline approach to account for modification due to bi-directional lateral loading. It was found that an increased reduction factor was needed in the resistance equations to be used to conduct a reliability analysis using Monte Carlo Simulation with MATLAB. A set of loops were programmed in the MATLAB program to compare the probability of failures of each mode and narrow down the exact failure mode at the end of each test.

This study found that more research needs to be done to help increase the accuracy of reliability analysis using Monte Carlo Simulation for Exposed Column Base Connections. The design guide one approach should be further checked against other experiments to help formulate an improved design guideline for base plate connections subjected to bi-directional lateral loading. It was found that one can predict the failure categories associated with column base connections through reliability analysis using Monte Carlo Simulation. Different loading scenarios should be checked with a more extensive test matrix to fully develop a program to measure a Column Base Connection System's reliability accurately. It is recommended to use a rod grade of at least grade 105 ksi standard (Fu=1010MPa) and ensure the base plate is thick enough to resist flexural yielding long enough for the column to buckle.

Chapter 7 Conclusions and Future Work

7.1 Summary

Four large-scale experiments were conducted to investigate the behaviour of exposed column base plate connections when subjected to combined axial and bi-directional lateral loading. All four experiments experienced anchor rod yielding as the main failure mode due to under sizing of the rods. All four experiments are categorized as Weak Connection / Strong Column failures where the connection fails before the column can reach its peak design values.

It was found that the 8-bolt configuration can resist base plate uplift more effectively than the 4-bolt configuration. The 8-bolt configuration has a greater moment capacity in both the major and minor directions when compared to the 4-bolt pattern. The inner rods of an 8-bolt pattern will greatly strengthen a connection depending on which axis they are located to reinforce. If the rods are added parallel to the major axis of the column, the rods will be engaged after the outer rods and will yield a cycle after the outer rods. If the rods are located perpendicular to the major axis of the column, they will be engaged before the outer rods and yield sooner. This in turn, will greatly strengthen the connection to resist uplift and base moment. It is recommended to locate the additional anchors perpendicular to the major axis to better resist any lateral loadings applied along the major axis. If the rods are located parallel to the major axis the inner rods are not able to effectively resist the forces generated in the major direction in unison with the outer rods. There is a reduction based on the distance between the outer rod and inner rod that must be accounted for when using additional rods which run parallel to the major loading axis.

It is of significant importance to design a connection with adequate anchor rod grade and baseplate configuration to achieve optimum failure. Safety is of great concern for a base connection where the column has been designed to resist bi-axial bending in both the major and minor axes. Anchor rod grade and diameter play a key role in the design of a base connection. It is recommended to not use less than a F1554 grade 105 ksi rod (F_y of 786 MPa) when designing a base connection to meet uplift conditions. Larger/taller column sections require additional rods with increased diameter, and adequate base plate thickness to achieve a Weak Column/ Strong Connection failure mode where the peak design values of the column can be achieved (plastic moment capacity).

Fahmy‘s (1999) Connection Strength Ratio works well for selecting a base plate configuration to meet the plastic moment capacity of a column, further investigation is required to check against combined axial and bi-axial bending. Design guide one RSB method is a useful method for calculating the tension demand for the anchor rods, and should be used when designing a CBP connection to resist uplift. The Eurocode column base rigidity check was found to be inadequate for designing CBP connections subjected to combined axial and bi-axial bending, where more work needs to be done to account for the baseplate and anchor rods into the base connection check. MCS Reliability Analysis can be utilized to categorize the specific failure modes of various CBP connections to help provide insight into designing a strong CBP connection. An exposed column base connection design should account for both major and minor directions, similar to a column design, to ensure that the column can fail as intended and safety of the system is achieved.

7.2 Conclusions

The following conclusions can be made from this experimental study:

- All experimental specimens (4-Bolt and 8-Bolt parallel) are categorized as Strong Column / Weak Connection failures where the connection fails before the column can reach its peak design values.
- All experimental specimens experience anchor rod yielding as the primary failure mode due to the under-sizing of the anchor rods.
- The 8-Bolt (parallel) configurations used in testing can resist base plate uplift more effectively than the 4-bolt configuration. The 8-bolt configurations have greater moment capacities in both the major and minor directions when compared to the 4-bolt bolt configurations.
- Additional anchor rods should be located perpendicular to the major axis of loading in order to ensure adequate tension resistance. A reduction is required when locating the rod within the depth of the column.
- Anchor rods used in CBP connection design where an uplift condition is present, should be sized accordingly to resist the tension force demand required to engage the plastic moment of the column before the connection fails. It is recommended to use F1554 grade 105 ksi (F_u

= 1010 MPa) as the minimum grade for anchor rod design. The diameter of the anchor rods should be very close to the thickness of the base plate if a strong connection is desired.

- Base plate thickness is a very decisive factor in CBP connection design. A base plate should be sized accordingly to resist the flexural demand of the connection, where the plastic moment of the column should be taken into consideration.
- Fahmy‘s Connection Strength ratio is a very effective method to design CBP connections to resist the uplift condition caused by lateral loading. The ratio classifies all the experimental specimens as weak connections which are true to the experimental outcome. The ratio also verifies a FEM CBP strong connection (FEM 7) which was used in the reliability analysis.
- Design Guide One Rectangular Stress Block method is an effective method for calculating the tension force demand for the anchor rods in a CBP connection subjected to combined axial loading and moment.
- Column Base Rigidity checks need to be modified to account for the contribution of the anchor rods and base plate, in order to be used effectively in CBP connection design.
- A MCS Reliability analysis was conducted which successfully classifies specific CBP connection failure modes for various 4-Bolt configurations based on experimental and FEM results. The reliability analysis found that the resistance factors used for the steel components in the connection (column, base plate, and anchor rods) require a modified reduction factor of 0.6 to account for the combined axial load and bi-directional lateral loading. It was found that the plastic moments in the column were engaging sooner and with less force due to the combined loading.
- A Strong Connection / Weak Column failure would have been achieved by using a 38mm thick base plate (same as Test 2 and 4) paired with 32mm diameter F1554 anchor rods (F_u = 1010 MPa) with the remaining components (column, weld, grout, concrete, etc.) the same as the experimental tests.

7.3 Recommendation for Future Work

It is recommended to do further testing into the behaviour of CBP connections subjected to combined axial and bi-directional lateral loading. Experimental results for a strong CBP connection would provide great insight into design of these connections. It is recommended to redo Test 2 and 4 with 32mm diameter F1554 anchor rods to achieve Strong Connection / Weak Column failure where the column buckles before the connection fails. With the results from a strong connection, current design guidelines can be further checked to assess how effective the design procedures are when subjected to combined axial and bi-axial bending.

It is recommended to test other sections such as larger/taller W sections or HS sections to analyze the connection behaviour and make proper comparisons. Different bolt configurations should be checked, such as 6-Bolt and 8-Bolt (perpendicular to major lateral loading). It is also recommended to test different bi-directional lateral loading protocols to observe the effects of increasing drift in the minor axis. A large-scale FEM CBP connection parametric study should be conducted which investigates various CBP connection configurations. Further investigation is required into CBP connection reliability analysis. Different design procedures such as Triangular Stress Block, and Connection Strength Ratio should be checked using similar reliability analysis techniques presented in this study.

References

Adany, S., Calado, L., and Dunai, L. (2000), "Experimental Studies on Cyclic Behavior Modes of Base Plate Connections," *Proceedings of the Third International Conference STESSA 2000* Montreal, Canada.

Akiyama, H., Kurosawa, M., Wakuni, N., and Nishinura, I. (1984), "Strength and Deformation of Exposed Type of Steel Column Bases," *Journal of Structural and Construction Engineering*, Transactions of AIJ, No. 342, pp. 46-54.

Akiyama, H., Yamada, S., Takahashi, M., Katsura, D., Kumura, K., and Yahata, S. (1998), "Full Scale Shaking Test of the Exposed-Type Column Bases," *Journal of Structural and Construction Engineering*, Transactions of AIJ, No. 514, pp. 185-192.

Architectural Institute of Japan (AIJ). (2001). Recommendations for Design of Connections in Steel Structures. Architectural Institute of Japan, Tokyo, Japan.

Astaneh, A., Bergsma, G., and Shen J.H. (1992), "Behavior and Design of Base Plates for Gravity, Wind and Seismic Loads," *Proceedings of the National Steel Construction Conference*, Las Vegas, Nevada, AISC, Chicago, Illinois.

Astaneh-Asl, A., Bergsma, G. (1993), "Cyclic Behavior and Seismic Design of Steel Base Plates," *Proceedings, Structures Congress*, ASCE 1993; 409–14.

Astaneh-Asl, A. (2008), "Seismic Behavior and Design of Base Plates in Braced Frames," *SteelTIPS*, Technical Information and Product Service, Structural Steel Educational Council.

ASTM Standard A307. (2007), "Standard Test Methods and Definitions for Mechanical Testing of Steel Products," *ASTM International*, West Conshohocken, PA.

Aviram, A., Stojadinovic, B., and Kiureghian, A. (2010). Performance and reliability of exposed column base plate connections for steel moment resisting frames. PEER Rep. 2010/107, Pacific Earthquake Engineering Research Center, Berkeley, CA, USA.

Borzouie, J. (2016). Low Damage Steel Base Connections. PhD Thesis, Department of Civil and Natural Resources Engineering, University of Canterbury, Christchurch, New Zealand.

Burda, J.J., and Itani, A.M. (1999), "Studies of Seismic Behavior of Steel Base Plates," Report No. CCEER 99-7, Reno (NV): Center of Civil Engineering Earthquake Research, Department of Civil and Environmental Engineering, University of Nevada, NV.

Canadian Institute of Steel Construction (CISC). (2014), "Handbook of Steel Construction Manual,"11th Edition, Canadian Institute of Steel Construction, Canada.

Chaboche, J. L. (2008). A review of some plasticity and viscoplasticity constitutive theories. International Journal of Plasticity, 24(10): 1642–1693.

Choi, J. H., and Choi, Y. (2013). "An experimental study on inelastic behavior for exposed-type steel column bases under three-dimensional loadings." J. Mech. Sci. Tech., 27(3), 747-759

Cloete, R. and Roth, C.P. (2021). "Column base connections under compression and biaxial moments: Proposed design approach." Journal of Constructional Steel Research, 184: 106814

CSA. (2019). Design of Steel Structures. CSA-S16-19, Canadian Standards Association, Toronto, ON, Canada.

CSA. (2019). Design of Concrete Structures. CSA-A23.3, Canadian Standards Association, Mississauga, ON, Canada.

Cui, Y., Nagae, T., and Nakashima, M. (2009), "Hysteretic Behavior and Strength Capacity of Shallowly Embedded Steel Column Bases" *ASCE Journal of Structural Engineering*.

Deng, J. (2023), "Lecture 18 – Simulation Techniques Ch.9: Monte Carlo Simulation Procedure" *ECIV 5110 Structural Reliability, Lakehead University*.

DeWolf JT, Sarisley EF. (1980). "Column base plates with axial loads and moments". *J Struct Div, ASCE 1980;106(11):2167–84*.

Drake RM, Elkin SJ. (1999). "Beam-column base plate design - LRFD method" *Eng J, AISC 1999;36(1):29–38.*

Di Sarno, L., Pecce, M.R., and Fabbrocino, G. (2006), "Inelastic Response of Composite Steel and Concrete Base Column Connections," Tokyo, STESSA 2006. Behavior of Steel Structures in Seismic Areas 2006. Mazzolani, F.M., editor. Published by A.A. Balkema, a member of Sweets & Zeitlinger Publishers, August 2006.

Elkady, A., and Lignos, D. G. (2014). "Modeling of the composite action in fully restrained beam-to-column connections: Implications in the seismic design and collapse capacity of steel special moment frames." J. Earthquake Eng. Struct. Dyn., 43(13), 1935–1954.

Elkady, A. (2016). "Collapse risk assessment of steel moment resisting frames designed with deep wide-flange columns in seismic regions." Ph.D. Dissertation, Department of Civil Engineering & Applied Mechanics, McGill University, Montreal, Quebec, Canada.

Eurocode 3. (2005). EN 1993-1-8; Design of steel structures – Part 1– 8: Design of Joints. CEN, European Committee for Standardization, Brussels, Belgium.

Fahmy, M., Stojadinovic, B., and Goel, S.C. (1999), –Analytical and Experimental Studies on the Seismic Response of Steel Column Bases," *Proceedings of the 8th Canadian Conference on Earthquake Engineering*.

Fahmy, M. (2000), –Seismic Behavior of Moment-resisting Steel Column Bases," Ph.D. Dissertation, Department of Civil and Environmental Engineering, University of Michigan, Ann Arbor, Michigan.

Fisher, J.M., and Kloiber, L.A. (2006). Design Guide 1: Base Plate and Anchor Rod Design. 2nd Ed. American Institute of Steel Construction (AISC), Chicago, USA.

Fasaee, M.A.K., Banan, M.R., Ghazizadeh, S. (2018), –Capacity of Exposed Column Base Connections Subjected to Uniaxial and Biaxial Bending Moments," J. Constr. Steel Res., 148, 368–370.

Gomez, I.R., Kanvinde, A.M., Smith, C., and Deierlein, G.G. (2009), –Shear Transfer in Exposed Column Base Plates," Technical Report submitted to the American Institute of Steel Construction, AISC, Chicago, IL.

Gomez, I., Deierlein, G., and Kanvinde, A., (2010). –Exposed column base connections subjected to axial compression and flexure." Final Rep. Presented to the American Institute of Steel Construction, Chicago.

Grauvilardell, J.E., Lee, D., Ajar, J.F., and Dexter R.J. (2005), –Synthesis of Design, Testing and Analysis Research on Steel Column Base Plate Connections in High Seismic Zones," Structural Engineering Report No. ST-04-02. Minneapolis (MN): Department of Civil Engineering, University of Minnesota.

Grigoriev, I.S., Meĭlikhov, E.Z., and Radzig, A.A. (1997). Handbook of Physical Quantities. CRC Press, Boca Raton, FL, 1997.

Hon, K.K., and Melchers, R.E. (1988). –Experimental Behavior of Steel Column Bases," *Journal of Constructional Steel Research*, Vol. 9, Paper No. 143, pp. 35-50.

Igarashi, S., Kadoya, H., Nakashima, S., and Suzuki, M. (1992), –Behavior of Exposed - Type Fixed Column Base Connected to Riser Foundation," *Proceedings of the Tenth World Conference on Earthquake Engineering*, Madrid, Spain.

Jaspart, J.P., and Vandegans, D. (1998), –Application of Component Method to Column Bases," *Journal of Constructional Steel Research*, Vol. 48, pp. 89-106.

Kallolil, J.J., Chakrabarti, S.K., and Mishra, R.C. (1998), "Experimental Investigation of Embedded Steel Plates in Reinforced Concrete Structures," *Engineering Structures*, Vol. 20, No. 1-2, pp. 105-112.

Kanvinde, A.M., and Deierlein, G.G. (2004), "Micromechanical Simulation of Earthquake Induced Fractures in Steel Structures," TR-145, John A. Blume Earthquake Engineering Center, Stanford University, CA.

Kanvinde, A., Grilli, D., and Zareian, F. (2012). "Rotational stiffness of exposed column base connections: Experiments and analytical models." J. Struct. Eng., 10.1061/(ASCE)ST.1943-541X.0000495, 549–560.

Kanvinde, A. M., Jordan, S. J., and Cooke, R. J. (2013). "Exposed column baseplate connections in moment frames—Simulations and behavioral insights." J. Constr. Steel Res., 84, 82–93.

Kanvinde, A. M., Higgins, P., Cooke, R. J., Perez, J., and Higgins, J. (2014). "Column base connections for hollow steel sections: Seismic performance and strength models." J. Struct. Eng., 10.1061/(ASCE) ST.1943-541X.0001136, 04014171.

Kim, S.E., Lee, D.H., and Cuong, N.H. (2007), "Shaking Table Tests of a Two-Story Unbraced Steel Frame," *Journal of Constructional Steel Research*, Volume 63, Issue 3, March 2007, Pages 412-421.

Krawinkler, H. (1996). "Cyclic loading histories for seismic experimentation on structural components." Earthquake Spectra, 12(1), 1–12.

Krawinkler, H. (2009). "Loading histories for cyclic tests in support of performance assessment of structural components." Proc., 3rd Int. Conf. on Advances in Experimental Structural Engineering, Pacific Earthquake Engineering Research Center, San Francisco.

Lee, D., and Goel, S.C. (2001). "Seismic Behavior of Column-Base Plate Connections Bending about Weak Axis," Report No. UMCEE 01-09, Department of Civil and Environmental Engineering, University of Michigan, Ann Arbor, Michigan.

Lee, D., Goel, S.C., and Stojadinovic, B. (2002), "Relative Strength Effects on Seismic Behavior of Column-Base Plate Connections under Weak Axis Bending," *Proceedings of the Seventh U.S. National Conference on Earthquake Engineering*, EERI, Boston, Massachusetts.

Lee, D.Y., Goel, S.C. and Stojadinovic, B. (2008a). Exposed Column-Base Plate Connections Bending about Weak Axis: I. Numerical Parametric Study. International Journal of Steel Structure, KSSC, 8(1): 11–27.

Li, T., Sakai, J., and Matsui, C. (2000), –Seismic Behavior of Steel-Concrete Composite Column Bases," *Proceedings of the 12th World Conference on Earthquake Engineering*, Paper 1072.

Liu T.C. (2001), –Investigation of Rotational Characteristics of Column _Pinned' Bases of Steel Portal Frames," *Steel and Composite Structures*, Vol. 1, No. 2, 187-200.

Lim, W.Y., Lee, D. and You, Y.C. (2017). –Cyclic loading tests on exposed column-base plate weak-axis connections of small-size steel structures." Engineering Structures, 153:653-664

Manjunath G. S., Dr.K Manjunath, & Sandeep, K. (2015). –Probability Failure of Column in Steel Structure". Retrieved from http://www.irjet.net/.

Melchers, R.E. (1992), –Column-Base Response under Applied Moment," *Journal of Constructional Steel Research*, Vol. 23, pp. 127-143.

Miyasaka, H., Arai, S., Uchiyama, M., Yamada, T., and Hashimoto, A. (2001), –Elasto-Plastic Behavior of Structural Elements Consist in Exposure Fixed-Type Steel Column Base. Part I – Behavior to Bending Moment," *Journal of Structural and Construction Engineering*, Transactions of AIJ, No 550, December 2001, pp.167-174.

Myers, A.T., Kanvinde, A.M., Deierlein, G.G., and Fell B.V. (2009), –Effect of Weld Details on the Ductility of Steel Column Baseplate Connections," *Journal of Constructional Steel Research*, Volume 65, Issue 6, June 2009, Pages 1366-1373.

Picard, A., Beaulieu, D., and Perusse, B. (1987), –Rotational Restraint of a Simple Column Base Connection," *Canadian Journal of Civil Engineering*, Vol. 14, pp.49-57.

SAC Joint Venture (1994). –SAC Steel Project". from https://www.sacsteel.org/.

Sato, K. (1987), –A Research on the Aseismic Behavior of Steel Column Base for Evaluating Its Strength Capacity and Fixity," Report No. 69, Kajima Institute of Construction Technology, Tokyo, Japan.

Seco, L., Couchaux, M., Hjiaj, M. and Neves, L.C. (2021). –Column base-plates under biaxial bending moment." Engineering Structures, 231:111386.

Somiya, Y., Fukuchi, Y., and Chin, B. (2002), –Experimental Study on Elasto-Plastic Behavior and Strength Estimation of Exposed-Type Column Base with Variable Axial Force," *Journal of Structural and Construction Engineering*, Transactions of AIJ, No. 562, pp. 137-143.

Song, B; Galasso, C; Kanvinde, A; (2021) –Reliability Analysis and Design Considerations for Exposed Column Base Plate Connections Subjected to Flexure and Axial Compression".

Journal of Structural Engineering, 147 (2), Article 04020328. 10.1061/(ASCE)ST.1943-541X.0002903

Sousa, A.C., Inamasu, H., and Lignos, D.G. (2020). An Explicit Model for Exposed Column Base Connections and its Parameter Sensitivity. Proceeding of 12th Pacific Structural Steel Conference, Tokyo, Japan.

Shaheen, M.A., Tsavdaridis, K.D., Salem, E. (2017), –Effect of Grout Properties on Shear Strength of Column Base connections: FEA and Analytical Approach," Engineering Structures, Volume 152, pp 307–319.

SIMULIA Inc. (2020). ABAQUS user's manual. Version 6.20. Providence, RI, USA.

Takamatsu, T., and Tamai, H. (2005), –Non-Slip-Type Restoring Force Characteristics of an Exposed-Type Column Base" *Journal of Constructional Steel Research*, Volume 61, Issue 7, July 2005, Pages 942-961.

Thambiratnam, D.P., and Paramasivam, P. (1986), –Base Plates Under Axial Loads and Moments," *Journal of Structural Engineering*, ASCE, Vol. 112, No. 5, pp. 1166-1181.

Targowski, R., Lamblin, D., and Guerlement, G. (1993), –Base Plate Column Connection under Bending: Experimental and Numerical Study," *Journal of Constructional Steel Research*, Vol. 27, pp. 37-54.

Trautner, C., and Hutchinson, T. (2013). –Structural base plate connection component testing—Phase I." SSRP-2013/07 and SSRP 2013/08, Univ. of California, San Diego.

Trautner, C., and Hutchinson, T. (2014). –Structural base plate connection component testing—Phase II." SSRP-2014/14 and SSRP 2014/15, Univ. of California, San Diego.

Trautner, C., Hutchinson, T., Grosser, P., and Silva, J. (2015). –Effects of detailing on the cyclic behavior of steel baseplate connections designed to promote anchor yielding." J. Struct. Eng., 10.1061/(ASCE)ST.1943-541X.0001361, 04015117.

Trautner, C. A., and Hutchinson, T. C. (2018). Parametric Finite-Element Modeling for Exposed Steel Moment Frame Column Baseplate Connections Subjected to Lateral Loads. ASCE Journal of Structural Engineering, 144(6): 04018049.

Zareian, F., and Kanvinde, A. (2013). Effect of column-base flexibility on the seismic response and safety of steel moment-resisting frames. Earthquake Spectra, 29(4): 1537–1559

Appendix A

Appendix A contains the stress vs. strain material property curves for the steel components used in experimental testing.

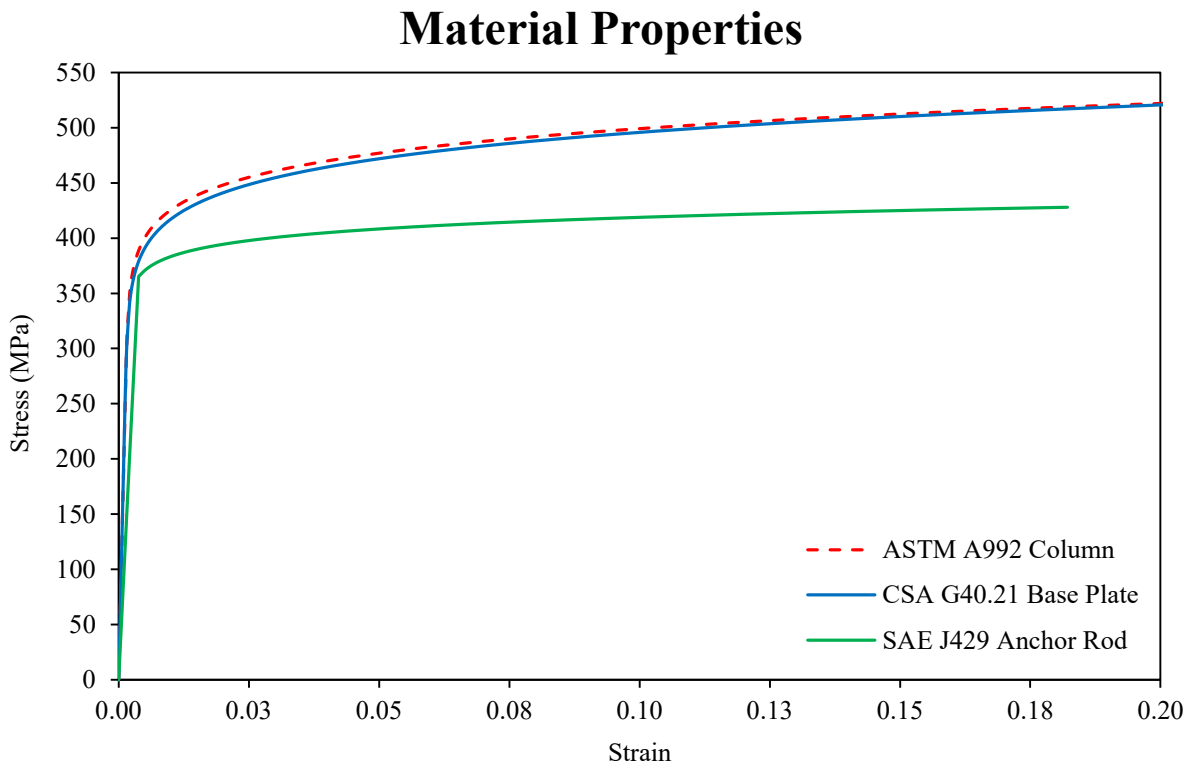

Appendix B

Appendix B contains additional actuator connection details.

Actuator Connection

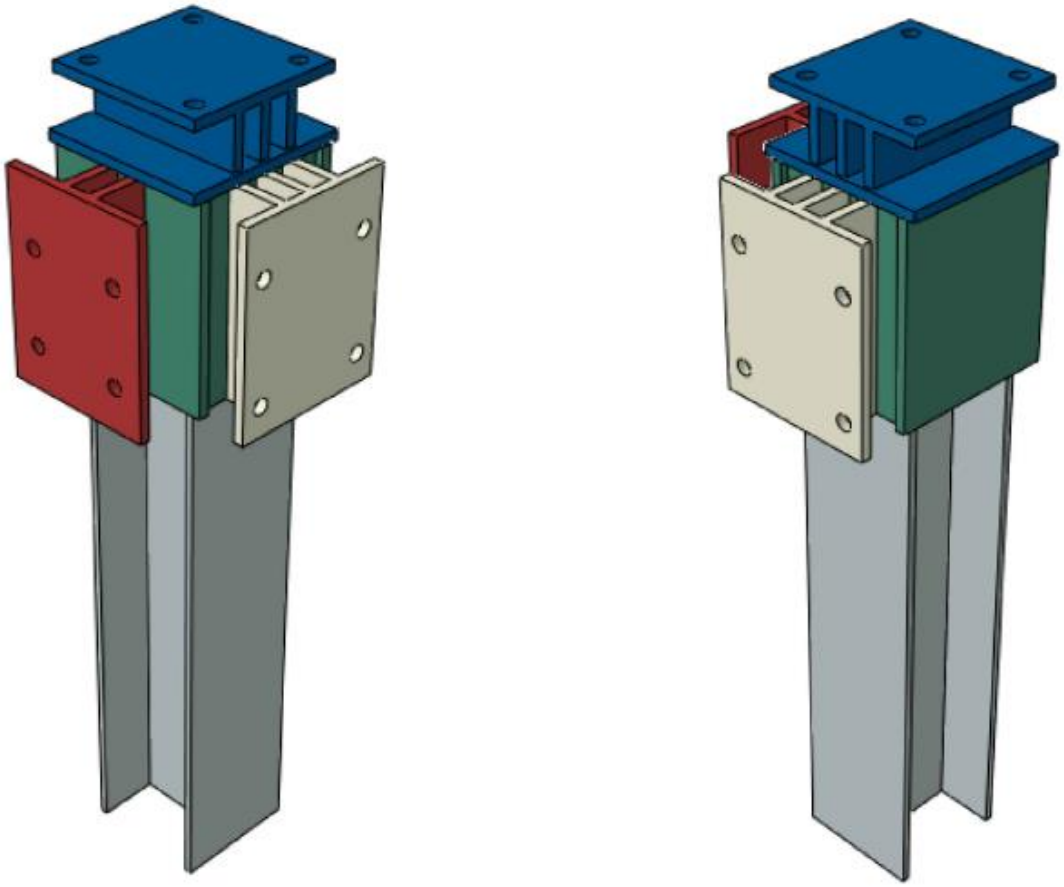

WELD DETAIL VERTICAL CORNER WELDS

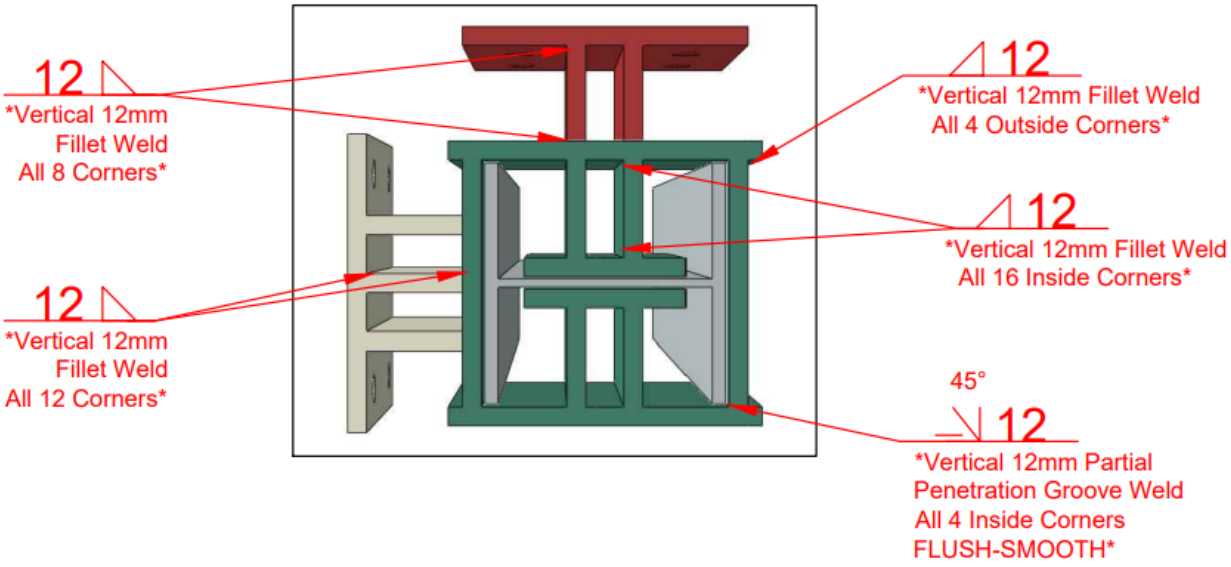

WELD DETAIL HORIZONTAL TOP PLATE PERIMETER

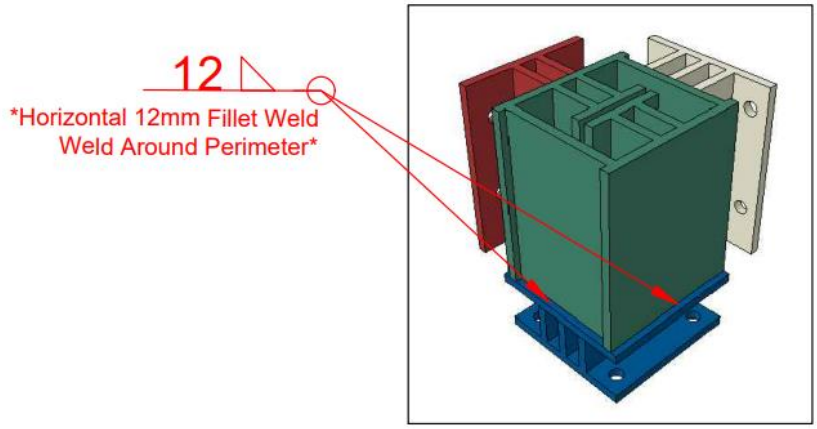

WELD DETAIL HORIZONTAL TOP PLATE SPACERS

12

*Horizontal 12mm Fillet Weld
Weld All 12 Corners*

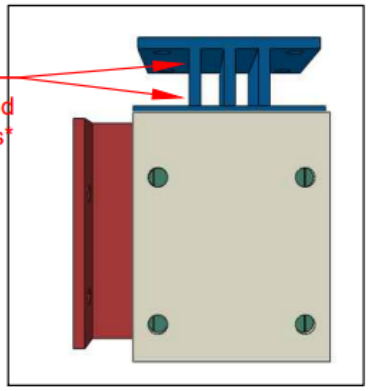

WELD DETAIL HORIZONTAL TOP PLATE

12

*Horizontal 12mm Fillet Weld
All 4 L-Shapes - Do Not Weld
Where Column Web Fits*

45°
12

*Horizontal 12mm Partial
Penetration Groove Weld
FLUSH-SMOOTH*

12

*Horizontal 12mm Fillet Weld
Stay 20mm away from corners*

12

*Horizontal 12mm Fillet Weld
Inside Edge Perimeter*

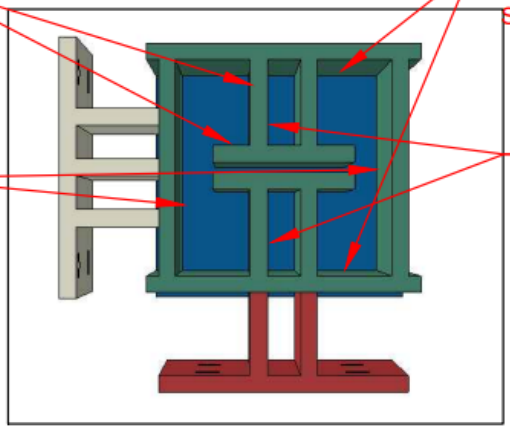

Appendix C

Appendix C contains the MATLAB code used to convert the anchor rod strain gauge readings into axial forces.

```
!x = ref microstrain from tension test !y is the ref Axial Force in kN

x = [-3824                                  y = [-103.403
0                                           0.000
3824                                        103.403
4143                                        103.937
4655                                        104.661
5270                                        105.386
6008                                        106.111
6895                                        106.836
7958                                        107.560
9232                                        108.285
10758                                       109.010
12582                                       109.735
14762                                       110.459
17365                                       111.184
20469                                       111.909
24168                                       112.634
28570                                       113.358
33804                                       114.083
40020                                       114.808
47396                                       115.533
56139                                       116.257
66492                                       116.982
78739                                       117.707
93212                                       118.432
110298                                      119.156
130449                                      119.881
154192                                      120.606
182140                                      121.331
200000]                                     121.351]


! x_course is the strain recorded during the experiment

x_course = []

!y_course = Axial Force in Anchor Rod

y_course = interpn(x,y,[x_course])
```

Appendix D

Appendix D contains the MCS Reliability Analysis MATLAB code used in Chapter 6.

```
%%%Reliability Analysis of Exposed Steel Column Base Connections%%%
%%%Using MONTE CARLO SIMULATION%%%
%%%Programed by KYLE ROLLER%%%

clear; clc;
t0=cputime;

%%%Random Variables%%%
%%% 12 RVs TOTAL for Geometry and Material Properties%%%

%%%Geometry%%%
%%%Units in mm%%%

%%%W250x73 ASTM A992 STEEL COLM%%%

Dc=253; %%%Depth of Colm%%%
cOvDc=0.002; %%%NORM DIST%%%
sigmaDc=(cOvDc*Dc);

Bf=264; %%%Flange Width%%%
cOvBf=0.004; %%%NORM DIST%%%
sigmaBf=(cOvBf*Bf);

Tf=14.2; %%%Flange Thickness%%%
cOvTf=0.025; %%%NORM DIST%%%
sigmaTf=(cOvTf*Tf);

Tw=8.6; %%%Web Thickness%%%
cOvTw=0.025; %%%NORM DIST%%%
sigmaTw=(cOvTw*Tw);

%%% CALC h after %%% CISC h=224.6 %%% Dc-(2 x Tf)%%%


%%%Base Plate CSA G40.21 (300W)%%%

Bp=406.4; %%%BP Length and Width (SQUARE)%%%
cOvBp=0.025; %%%NORM DIST%%%
sigmaBp=(cOvBp*Bp);

Bg=38;    %%%BP EDGE DISTANCE to ROD CENTER (g typically)%%%
cOvBg=0.05; %%%NORM DIST%%%
sigmaBg=(cOvBg*Bg);

BTf=38; %%%BP Thickness (CHANGE FOR DIFFERENT TESTS)%%%
cOvBTf=0.03; %%%NORM DIST%%%
sigmaBTf=(cOvBTf*BTf);


%%%ANCHOR RODS%%%

Dr=32; %%%DIAMETER of ROD (CHANGE FOR TESTS)%%%
cOvDr=0.085; %%%NORM DIST%%%
sigmaDr=(cOvDr*Dr);
```

```
%%%MATERIAL PROPERTIES%%%

%%%COLM-ASTM A992-(MPa)%%%
CFy=390; %%%Yield Strength of COLM%%%
cOvCFy=0.05; %%%NORM DIST%%%
sigmaCFy=(cOvCFy*CFy);

%%%BasePlate-300W-(MPA)%%%
BFy=366; %%%Yeild Strength%%%
cOvBFy=0.07; %%%NORM DIST%%%
sigmaBFy=(cOvBFy*BFy);

%%%Concrete-(MPa)%%%
fc=32.7; %%%Comp Strength%%%
cOvfc=0.145; %%%NORM DIST%%%
sigmafc=(cOvfc*fc);

%%%Anchor Rod-(MPa)%%%-LOG-NORM%%%
RFu=1010; %%%Grade 105 ksi (CHANGE WITH TESTS)%%%
cOvRFu=0.16; %%% 0.16 for Grade 36 ksi and 0.09 for Grade 105 ksi%%% (CHANGE FOR↙
TESTS)%%%
initialsigma=RFu*cOvRFu; %%%Std Dev
vRFu= initialsigma^2; %%%Variance

%%%LOG-NORM so need to get LOG-NORM variables%%%

lambdaRFu=log((RFu^2)/sqrt(vRFu+RFu^2)); %%%LOG-NORM%%%
sigmaRFu=(sqrt(log(vRFu/(RFu^2)+1)));


%%%MCS-RANDOM NUMBER GENERATOR FOR 12 RVs%%%

nS=10^6; %%% NUMBER OF RUNS%%%

%%%Four Performace Equations - ONES%%%
ig1=ones(nS,1);
ig2=ones(nS,1);
ig3=ones(nS,1);
ig4=ones(nS,1);

%%%RANDOM NUMBERS%%%

%%%COLM GEOMETRY%%%
x1=(normrnd(Dc,sigmaDc,nS,1)); %%%Dc
x2=(normrnd(Bf,sigmaBf,nS,1)); %%%Bf
x3=(normrnd(Tf,sigmaTf,nS,1)); %%%Tf
x4=(normrnd(Tw,sigmaTw,nS,1)); %%%Tw

%%%BP GEOMETRY%%%
x5=(normrnd(Bp,sigmaBp,nS,1)); %%%Bp
x6=(normrnd(Bg,sigmaBg,nS,1)); %%%BP
x7=(normrnd(BTf,sigmaBTf,nS,1)); %%%BTf

%%%ROD GEOMETRY%%%
x8=(normrnd(Dr,sigmaDr,nS,1)); %%%Dr
```

```
%%%MATERIAL PROPS%%%
x9=(normrnd(CFy,sigmaCFy,nS,1)); %%%CFy
x10=(normrnd(BFy,sigmaBFy,nS,1)); %%%BFy
x11=(normrnd(fc,sigmafc,nS,1)); %%%fc
x12=(lognrnd(lambdaRFu,sigmaRFu,nS,1)); %%%lambdaRFu


%%%Performace Equations for Failure Modes%%% (Z = R - S)%%%


%%%COLM%%%
h=(x1(:)-(2.*(x3(:)))); %%%h = Dc-(2*Tf)%%%
A=((2.*(x2(:).*x3(:)))+(h(:).*x4(:))); %%%Cross Sect Area

%%%Centroids of Half Sections%%%
Zxbar=(((x2(:).*x3(:)).*((x3(:)./2)+(h(:)./2)))+(((h(:)./2).*x4(:)).*h(:)./4))./((x2(:).↙
*x3(:))+((h(:)./2).*x4(:)));

Zybar=(((2.*((x2(:)./2).*x3(:).*(x2(:)./4)))+((h(:).*(x4(:)./2).*(x4(:)./4)))./((2.*((x2↙
(:)./2).*x3(:)))+((h(:).*(x4(:)./2)))));

%%%PLASTIC SECTION MODULUS%%%
Zx=(A(:).*Zxbar(:));
Zy=(A(:).*Zybar(:));

%%%Plastic Moment Resistance in Both X and Y Directions%%% (Mp = Fy x Z)%%%
CMrx=(((x9(:).*Zx(:))*10^-6).*0.60); %%%COLM PLASTIC MOMENT RESISTANCE MAJOR in kN x m%%%
CMry=(((x9(:).*Zy(:))*10^-6).*0.60); %%%COLM PLASTIC MOMENT RESISTANCE MINOR in kN x m%%%
%%%RESISTANCE FACTOR OF 0.60 added%%%%

MxMax=233.3; %%%units in kNxm %%% (CHANGE EACH TEST ACCORDING TO EXPERIMENTAL AND FEM↙
RESULTS RESULTS)
MyMax=122.6;%%%units in kNxm %%% (CHANGE EACH TEST ACCORDING TO EXPERIMENTAL AND FEM↙
RESULTS RESULTS)


%%%COLM PERFORMANCE EQUATIONS%%

%%%MAJOR%%%
g1=(CMrx(:)-MxMax); %%% Z = R - S
nF1=sum(ig1(g1<0));
pF1=nF1/nS;
pF1B=(pF1-1)*-1;

Beta1=(norminv(pF1B)); %%% RELIABILTY INDEX - Major Column Buckling

%%%MINOR%%%
g2=(CMry(:)-MyMax);
nF2=sum(ig2(g2<0));
pF2=nF2/nS;
pF2B=(pF2-1)*-1;

Beta2=(norminv(pF2B)); %%% RELIABILTY INDEX - Minor Column Buckling

%%%ROD PERFORMANCE EQUATION BUILDING%%%
%%%Design Guide One Approach for Demand%%%
```

```
fmax=(1.7*0.65.*x11(:)); %%%Concrete Bearing Stress - Less than 1.7 fc' - 0.65 reduction factor%%%%

Mmax=281; %%% Max COMBINED MOMENT kN x m - Taken from Experiments/Analysis %%%% (CHANGE PER TEST)

P=400; %%%Axial Load in kN

%%%ROD TENSION FORCE DEMAND%%%
RTf=((fmax(:).*(x5(:).*((x5(:)-x6(:))-((((x5(:)-x6(:)).^2)-((2.*((Mmax*10^6)+((P*10^3).* ((x5(:)./2)-x6(:))))))./((fmax(:).*x5(:))))).^0.5))))-(P*10^3))/1000;

%%%ROD TENSION RESISTANCE%%%
Ar=(pi.*((x8(:)./2).^2)); %%%Cross-Sect Area of Rod

RTr=((0.60*(0.85.*Ar(:)).*x12(:))./1000); %%%ROD Tension Resistance in kN - (Resistance factors x A x Fu)%%%
%%%ONE ROD ***MULTIPLY BY NUMBER OF RODS%%%
%%%RESISTANCE FACTOR CAHNGED FROM 0.67 to 0.60%%%

%%%ROD PERFORMANCE EQUATION%%% Z = R - S
g3=((2.*RTr(:))-RTf(:)); %%% 4-BOLT CONFIGURATION-MULTIPLY RTr by 2!!! %%%
nF3=sum(ig3(g3<0));
pF3=nF3/nS;
pF3B=(pF3-1)*-1;

Beta3=(norminv(pF3B)); %%% RELIABILTY INDEX - ROD YIELDING


%%% BP Performan Equation Building %%%
%%% Design Guide One Approach%%%

BMr=((((x10(:).*((x7(:).^2)))/4)*10^-3).*0.60); %%%Resistance in BP - (Mp = Fy x Z) %%% kN x m
%%%RESISTANCE FACTOR OF 0.60 added%%%

Yarm=((x5(:)./2)-x6(:)-(0.475.*x1(:))); %%%BP Lever Arm%%% Yarm = (Bp/2)-g-(0.475*Dc)%%%

BMf=((((RTf(:).*1000).*Yarm(:))./x5(:))*10^-3); %%%BP Flexural Demand per unit width of BP%%% kn x m

%%%BP PERFORMANCE EQUATION%%% Z = R - S
g4=(BMr(:)-BMf(:));
nF4=sum(ig4(g4<0));
pF4=nF4/nS;
pF4B=(pF4-1)*-1;

Beta4=(norminv(pF4B)); %%% RELIABILTY INDEX - BP YIELDING

%%%FAILURE CATEGORY%%%
if (pF1>pF2) && (pF1>pF3) && (pF1>pF4)
    disp('Colm Major Platic Moment Governs - Strong or Balanced Failure')

elseif (pF2>pF1) && (pF2>pF3) && (pF2>pF4)
    disp('Colm Minor Platic Moment Governs - Strong or Balanced Failure')
```

```
elseif (pF3>pF1) && (pF3>pF2) && (pF3>pF4)
    disp('Anchor Rod Yielding Governs - Weak or Balanced Failure')

elseif (pF4>pF1) && (pF4>pF2) && (pF4>pF3)
    disp('Base Plate Yielding Governs - Weak or Balanced Failure')
end


if (pF3>pF1) && (pF3>pF2) && (pF4>pF1) && (pF4>pF2) && (pF1<0.5) && (pF2<0.5)
    disp('Weak Connection - Rods and BP Yield')

elseif (pF3>pF1) && (pF3>pF2) && (pF1<0.5) && (pF2<0.5)
    disp('Weak Connection - Rods Yield')

elseif (pF4>pF1) && (pF4>pF2) && (pF1<0.5) && (pF2<0.5)
    disp('Weak Connection - BP Yield')
end

if (pF1>pF3) && (pF1>pF4) && (pF2>pF3) && (pF2>pF4) && (pF3<0.5) && (pF4<0.5)
    disp('Strong Connection - Colm Yield Major and Minor')

elseif (pF1>pF3) && (pF1>pF4) && (pF3<0.5) && (pF4<0.5)
    disp('Strong Connection Connection - Colm Yield Major')

elseif (pF2>pF3) && (pF2>pF4) && (pF3<0.5) && (pF4<0.5)
    disp('Strong Connection - Colm Yield Minor')
end

if (pF1>0.3) && (pF1>pF4) && (pF2>0.3) && (pF2>pF4) && (pF3>0.5) && (pF4>0.5)
    disp('Balanced Connection - Colm Yield Major and Minor + Rods + BP')

elseif (pF1>0.3) && (pF1>pF4) && (pF2>0.3) && (pF2>pF4) && (pF3>0.5) && (pF4<0.5)
    disp('Balanced Connection - Colm Yield Major and Minor + Rods')

elseif (pF1>0.3) && (pF1>pF4) && (pF2>0.3) && (pF2>pF4) && (pF3<0.5) && (pF4>0.5)
    disp('Balanced Connection - Colm Yield Major and Minor + BP')

elseif (pF1>0.3) && (pF1>pF2) && (pF3>0.5) && (pF4>0.5)
    disp('Balanced Connection - Colm Yield Major + Rods + BP')

elseif (pF1>0.3) && (pF1>pF2) && (pF3>0.5) && (pF4<0.5)
    disp('Balanced Connection - Colm Yield Major + Rods')

elseif (pF1>0.3) && (pF1>pF2) && (pF3<0.5) && (pF4>0.5)
    disp('Balanced Connection - Colm Yield Major + BP')

elseif (pF2>0.3) && (pF2>pF1) && (pF3>0.5) && (pF4>0.5)
    disp('Balanced Connection - Colm Yield Minor + Rods + BP')

elseif (pF2>0.3) && (pF2>pF1) && (pF3>0.5) && (pF4<0.5)
    disp('Balanced Connection - Colm Yield Minor + Rods')

elseif (pF2>0.3) && (pF2>pF1) && (pF3<0.5) && (pF4>0.5)
    disp('Balanced Connection - Colm Yield Minor + BP')
end
```